Research Paper

GEOSPHERE

GEOSPHERE

https://doi.org/10.1130/GES02294.1

15 figures; 4 tables; 1 set of supplemental files

CORRESPONDENCE: desilvas@geo.oregonstate.edu

CITATION: de Silva, S.L., Roberge, J., Bardelli, L., Báez, W., Ortiz, A., Viramonte, J.G., Arnosio, J.M., and Becchio, R., 2022, Magmatic evolution and architecture of an arc-related, rhyolitic caldera complex: The late Pleistocene to Holocene Cerro Blanco volcanic complex, southern Puna, Argentina: Geosphere, https://doi.org/10.1130/GES02294.1.

Science Editor: David E. Fastovsky
Guest Associate Editor: Lily Claiborne

Received 2 June 2020
Revision received 20 August 2021
Accepted 16 October 2021

Published online 25 January 2022

Magmatic evolution and architecture of an arc-related, rhyolitic caldera complex: The late Pleistocene to Holocene Cerro Blanco volcanic complex, southern Puna, Argentina

S.L. de Silva[1], J. Roberge[2], L. Bardelli[3], W. Báez[3], A. Ortiz[3], J.G. Viramonte[3], J.M. Arnosio[3], and R. Becchio[3]

[1]College of Earth, Ocean, and Atmospheric Science, Oregon State University, 104 CEOAS Admin, Corvallis, Oregon 97331, USA
[2]Escuela Superior de Ingeniería y Arquitectura (ESIA)–Ticomán, Instituto Politécnico Nacional (IPN), 07340 Mexico City, D.F., Mexico
[3]Instituto de Bio y Geociencias del *Noroeste Argentino* (IBIGEO, UNSa-CONICET), Avenida 9 de Julio 14, A4405BBA Salta, Argentina

ABSTRACT

Through the lens of bulk-rock and matrix glass geochemistry, we investigated the magmatic evolution and pre-eruptive architecture of the siliceous magma complex beneath the Cerro Blanco volcanic complex, a Crater Lake–type caldera complex in the southern Puna Plateau of the Central Andes of Argentina. The Cerro Blanco volcanic complex has been the site of two caldera-forming eruptions with volcanic explosivity index (VEI) 6+ that emplaced the ca. 54 ka Campo Piedra Pomez ignimbrite and the ca. 4.2 ka Cerro Blanco ignimbrite. As such, it is the most productive recent explosive volcano in the Central Andes. The most recent eruptions (younger than 4.2 ka) are dominantly postcaldera effusions of crystal-rich domes and associated small explosive pulses. Previous work has demonstrated that andesitic recharge of and mixing with rhyolitic magma occurred at the base of the magma complex, at ~10 km depth.

New isotopic data (Sr, Nd, Pb, and O) confirm that the Cerro Blanco volcanic complex rhyolite suite is part of a regional southern Puna, arc-related ignimbrite group. The suite defines a tight group of consanguineous siliceous magmas that serves as a model for the evolution of arc-related, caldera-forming silicic magma systems in the region and elsewhere. These data indicate that the rhyolites originated through limited assimilation of and mixing with upper-crustal lithologies by regional basaltic andesite parent materials, followed by extensive fractional crystallization.

Least squares models of major elements in tandem with Rayleigh fractionation models for trace elements reveal that the internal variations among the rhyolites through time can be derived by extensive fractionation of a quartz–two feldspar (granitic minimum) assemblage with limited assimilation. The rare earth element character of local volumes of melt in some samples of the Campo Piedra Pomez ignimbrite basal fallout requires significant fractionation of amphibole. The distinctive major- and trace-element characteristics of bulk rock and matrix of the Campo Piedra Pomez and Cerro Blanco tephras provide useful geochemical fingerprints to facilitate regional tephrochronology. Available data indicate that rhyolites from other neighborhood centers, such as Cueros de Purulla, share bulk chemical characteristics with the Campo Piedra Pomez ignimbrite rhyolites, but they appear to be isotopically distinct.

Pre-eruptive storage and final equilibration of the rhyolitic melts were estimated from matrix glass compositions projected onto the haplogranitic system (quartz-albite-orthoclase-H_2O) and using rhyolite-MELTS models. These revealed equilibration pressures between 360 and 60 MPa (~10–2 km depth) with lowest pressures in the Holocene eruptions. Model temperatures for the suite ranged from 695 to 790 °C.

Integrated together, our results reveal that the Cerro Blanco volcanic complex is a steady-state (low-magmatic-flux), arc-related complex, standing in contrast to the flare-up (high-magmatic-flux) supervolcanoes that dominate the Neogene volcanic stratigraphy. The silicic magmas of the Cerro Blanco volcanic complex were derived more directly from mafic and intermediate precursors through extensive fractional crystallization, albeit with some mixing and assimilation of local basement. Geochemical models and pressure-temperature estimates indicate that significant volumes of remnant cumulates of felsic and intermediate composition should dominate the polybaric magma complex beneath the Cerro Blanco volcanic complex, which gradually shallowed through time. Evolution to the most silicic compositions and final equilibration of some of the postcaldera domes occurred during ascent and decompression at depths less than 2 km.

Our work connotes an incrementally accumulated (over at least 54 k.y.), upper-crustal pluton beneath the Cerro Blanco volcanic complex between 2 and 10 km depth. The composition of this pluton is predicted to be dominantly granitic, with deeper parts being granodioritic to tonalitic. The progressive solidification and eventual contraction of the magma complex may account for the decades of deflation that has characterized Cerro Blanco. The presently active geothermal anomaly and hydrothermal springs indicate the Cerro Blanco volcanic complex remains potentially active.

Shanaka de Silva https://orcid.org/0000-0002-0310-5516

INTRODUCTION

The formation, evolution, and magma dynamics in rhyolitic volcanic systems are of great relevance to concerns about volcanic risk from potentially explosive eruptions. These themes are also central to addressing fundamental questions about the volcano-plutonic relationship, the construction of plutons and batholiths, and ultimately the formation of the continental crust. An understanding of the origin of rhyolites requires answers to questions about the relative roles of open versus closed systems, upper versus deeper crustal evolution, and differentiation mechanisms.

The Central volcanic zone of the Andes (CVZ) has one of the best-preserved records of siliceous volcanism on Earth. Two distinct groups of products have been identified: (1) Regional-scale ignimbrites from "supereruptions" (>450 km^3 dense rock or magma equivalent) such as those from nested resurgent caldera complexes like Cerro Galan, Argentina (Sparks et al., 1985; Folkes et al., 2011a), and those of the Altiplano-Puna volcanic complex (de Silva, 1989; de Silva et al., 2006; Salisbury et al., 2011), and (2) smaller-volume (<50 km^3) ignimbrites associated with smaller calderas and young composite cones of the Quaternary arc (Siebel et al., 2001; Kay and Coira, 2009; Naranjo et al., 2018). These two groups are chemically and isotopically distinct, with the small ignimbrites and associated centers having a cogenetic relationship with the andesites of the arc (Siebel et al., 2001; Schnurr et al., 2007; Goss and Kay, 2009; Goss et al., 2010), whereas the large dacitic supereruptions have more crustal affinity (de Silva, 1989; Francis et al., 1989; Lindsay et al., 2001; Schmitt et al., 2001; de Silva et al., 2006; Kay et al., 2010a, 2010b; Folkes et al., 2011c, 2013; Freymuth et al., 2015; Brandmeier and Wörner, 2016; Grocke et al., 2016; de Silva and Kay, 2018). The fundamental difference between these two groups is thought to be related to the thermal flux driving the magmatism (de Silva, 2008; de Silva and Gregg, 2014); supervolcanism is thought to be driven by high thermal flux from the mantle (flare-up) triggered by some major rearrangement of the crust-mantle interface (delamination, for instance; Kay and Coira, 2009; Freymuth et al., 2015; de Silva and Kay, 2018), whereas the smaller arc-related systems are driven by the background thermal flux (normal flux or steady state; Hildreth, 1981; de Silva, 2008) associated with magma production by subduction. A more complete perspective of these relationships requires detailed understanding of the timing, development, and eruptive fluxes of volcanic centers coupled to magma dynamics and evolution. While some progress toward this has been made for the larger systems (e.g., Lindsay et al., 2001; Schmitt et al., 2001; Folkes et al., 2011a, 2011b, 2011c; Wright et al., 2011; Grocke et al., 2017a, 2017b), little is known about the details of the smaller ignimbrites and their centers.

One of the most productive regions of this smaller-volume rhyolitic volcanism is the southern Puna Plateau region of Catamarca, Argentina (Fig. 1; Siebel et al., 2001; Kay and Coira, 2009; Goss et al., 2010). The broader regional context and magma genesis of these rhyolites are well understood, and it has been established that there are important differences between different groups of rhyolites. To the west of the Cerro Galan caldera complex, between 25°S and 27°S, Siebel et al. (2001) identified a Salar de Antofalla Group and a Salar de Isla group, corresponding to an east-west international split, with the former being in Argentina and the latter located in Chile. Siebel et al. (2001) argued for a strong affinity to composite-cone–forming andesites for the rhyolites through upper-crustal assimilation and fractional crystallization (AFC) processes. However, at the southern extreme of the Central volcanic zone, at the Incapillo caldera at ~28°S, Goss et al. (2010) emphasized the importance of deep crustal silicic magma genesis. Apart from the Incapillo caldera, the geochemistry of individual siliceous centers in the southern Puna has not been studied in any detail.

One of the most prolific centers in the southern Puna is the Cerro Blanco volcanic complex (Fig. 2), the source of two major rhyolitic eruptions previously dated at <73 ka and 4.2 ka, making it one of the youngest and most prolific siliceous volcanoes in the Central Andes (Arnosio et al., 2008; Montero Lopez et al., 2010a; Báez et al., 2015; Fernández-Turiel et al., 2019; Báez, 2020a, 2020b). Building on several decades of regional and local reconnaissance, recent work has now unraveled the eruptive history and volcanology of this spectacular and important center (Báez et al., 2020a, 2020b). This framework now allows the development of the magmatic system to be investigated. A notable feature is that the Cerro Blanco volcanic complex siliceous suite defines a coherent group that is distinct within the small, arc-related ignimbrites of Siebel et al. (2001) and Schnurr et al. (2007), and the Incapillo caldera of Goss et al. (2010). This motivated us to investigate the Cerro Blanco volcanic complex as a coherent silicic magmatic system that records the development and evolution of an arc-related rhyolitic magmatic complex in thick continental crust. With the foundation of well-understood field relations, stratigraphy, and geochronology, and new and previously available petrological and geochemical data, herein we provide the first model for the development of this silicic magma complex.

Our purpose here was to develop a new working model for the generation, evolution, and conditions of pre-eruption storage of the Cerro Blanco volcanic complex suite. Therefore, in this contribution, we investigated the following themes:

(1) the origin of the rhyolites as a distinct suite in the southern Puna;
(2) the relationships among the rhyolites of the Cerro Blanco volcanic complex;
(3) pressure-temperature (*P-T*) conditions of pre-eruptive storage and architecture of the magmatic complex; and
(4) the temporal evolution of the magma system.

We achieved this through new bulk chemical analyses of major and trace elements as well as radiogenic (Sr, Nd, and Pb) and stable (O) isotopes, in situ matrix glass chemistry (major and trace elements), and intensive parameters based on glass chemistry and MELTS modeling. These new data were combined with available data from the literature. We also obtained a new $^{40}Ar/^{39}Ar$ age of 54.6 ± 0.6 ka for the Campo Piedra Pomez ignimbrite eruption, which requires a recalibration of the temporal development of the Cerro Blanco volcanic complex.

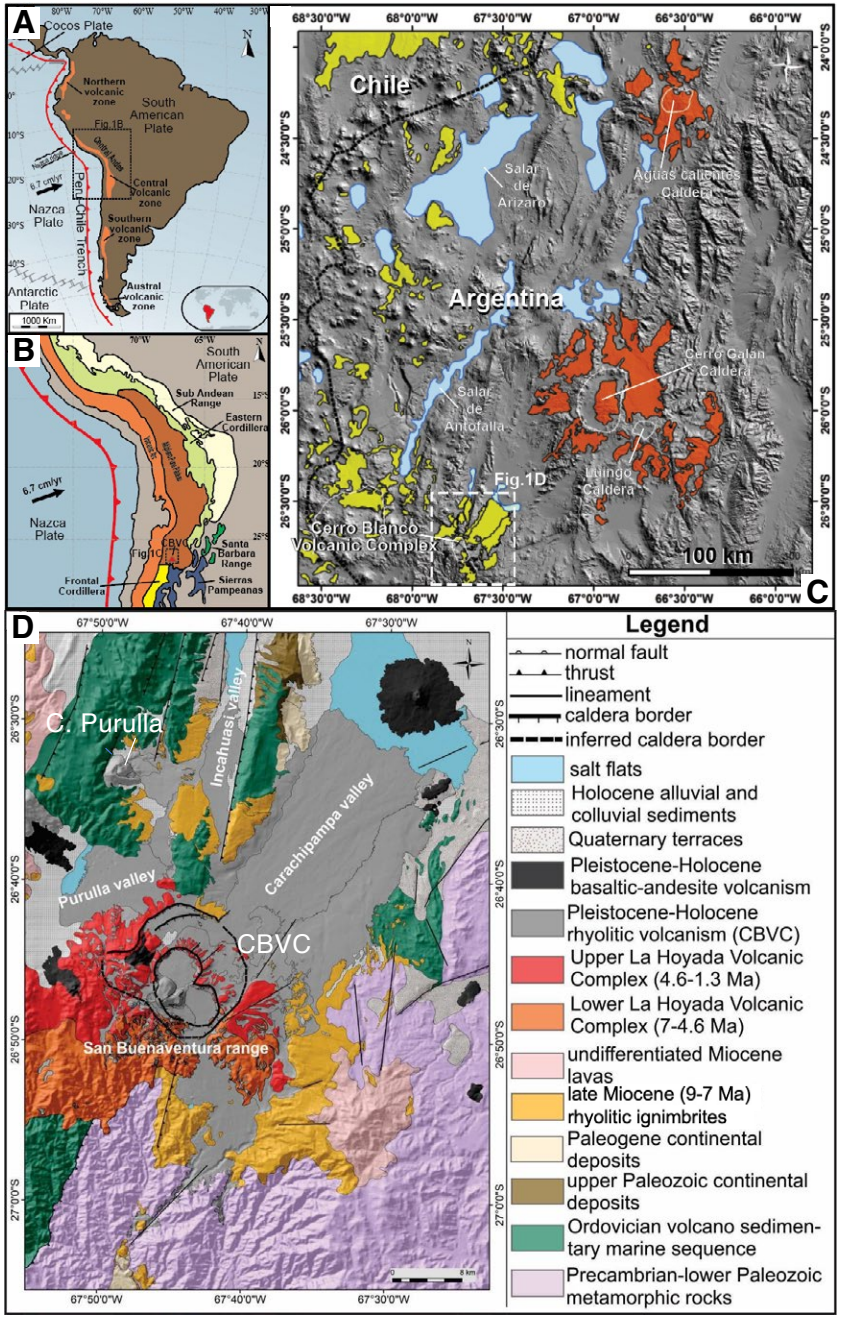

Figure 1. (A) Location of the Central volcanic zone (CVZ) in the geodynamic framework of South America (from Norini et al., 2014). (B) Main morpho-structural provinces in the Central Andes (from Norini et al., 2014); CBVC—Cerro Blanco volcanic complex. (C) Distribution of ignimbrites in the southern Puna region from Guzmán et al. (2014). Orange—crystal-rich dacitic ignimbrites; yellow—crystal-poor rhyolitic ignimbrites. The Catamarca province occupies the SE quadrant of this map. (D) Geological map of the study area (from Báez et al., 2020a, 2020b).

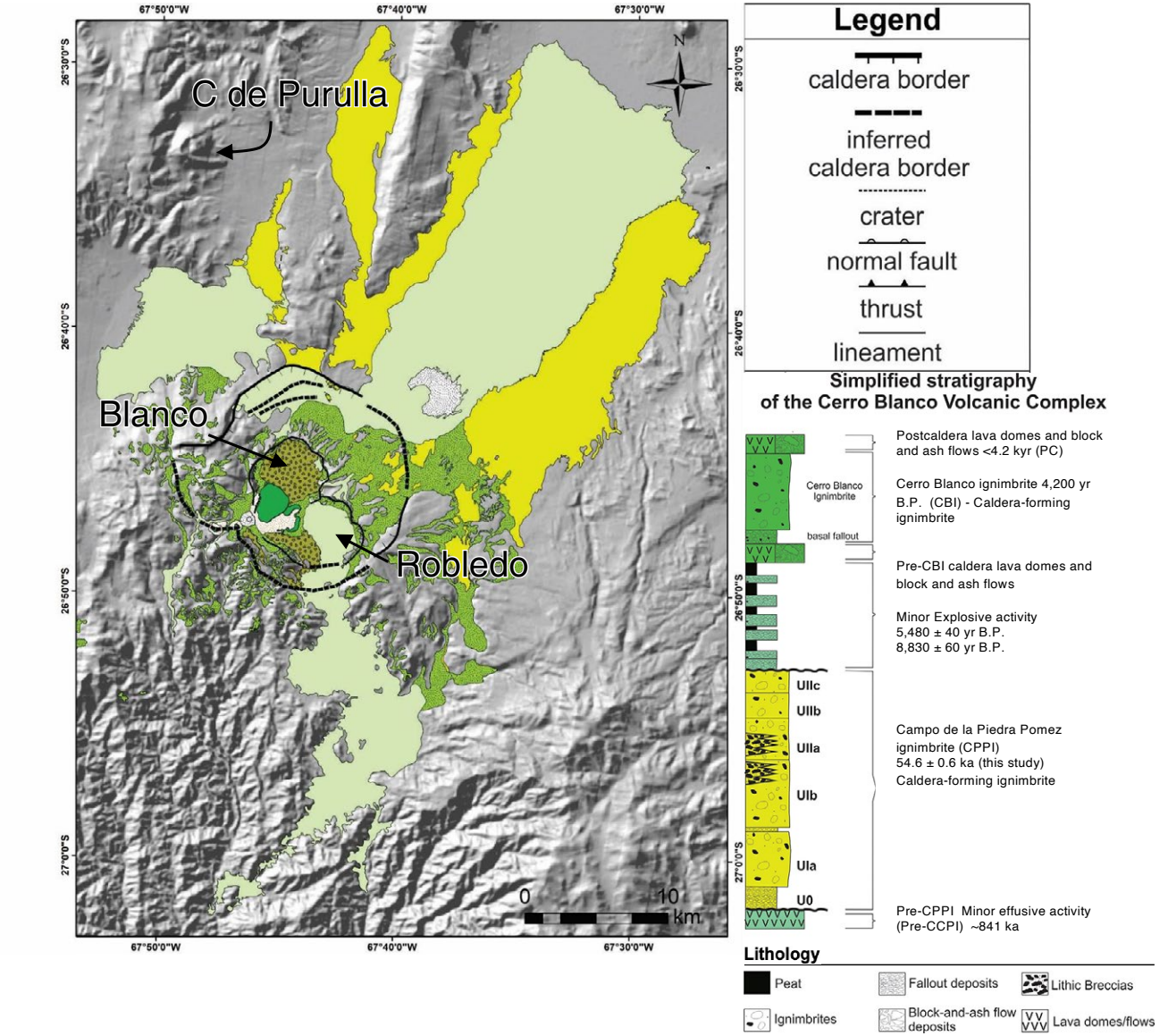

Figure 2. Geologic map Cerro Blanco volcanic complex (CBVC from Báez et al., 2020b), with schematic stratigraphic column presenting the main eruptive events of the late Pleistocene to Holocene history of the Cerro Blanco volcanic complex. For details of the internal stratigraphy of the Campo Piedra Pomez ignimbrite eruption, the reader is referred to Báez et al. (2020a). The details of the volcanology of the Cerro Blanco ignimbrite eruption can be found in Báez et al. (2020b). Ages for the minor explosive activity are from Montero López et al. (2009). The new age of 54.6 ± 0.6 ka for the Campo Piedra Pomez ignimbrite determined in this study is shown here. Other sources of age data are discussed in the main text.

GEOLOGICAL AND PETROCHEMICAL CONTEXT

Volcanism in the Puna Plateau

The subduction-related continental margin of the Andes is one of the most active volcanic regions on Earth, with four active volcanic regions (Fig. 1). The Central volcanic zone, which hosts the Cerro Blanco volcanic complex, is structurally and tectonically coupled to the Central Andes (Isacks, 1988; de Silva and Francis, 1991; Allmendinger et al., 1997). The main topographic feature in the Central Andes is the Altiplano-Puna, a high plateau upon which Neogene arc magmatism constructed the Central volcanic zone (Figs. 1A and 1B). The north-south–trending volcanic arc initiated in Neogene times, initially along the Maricunga belt and finally stabilizing 50 km to the west in the present-day volcanic arc (Western Cordillera; Kay and Coira, 2009; Guzmán et al., 2014). Shallowing of the subducting slab resulted in eastward broadening of arc magmatism along regional NW-SE–trending, vertical, strike-slip fault systems (e.g., Viramonte et al., 1984; Viramonte and Petrinovic, 1990; Petrinovic et al., 2006; Riller et al., 2001; Acocella et al., 2011). The Neogene section of the Central volcanic zone is characterized by the presence of significant volumes of crystal-rich silicic ignimbrites that form the Central Andean Neogene ignimbrite province, related to a spatiotemporally transgressive magmatic flare-up correlated, to a first-order, to the southward propagation of the subducting Juan Fernandez Ridge (Kay and Coira, 2009; Freymuth et al., 2015; de Silva and Kay, 2018). In Pleistocene–Holocene times, the southern sector of the Central volcanic zone (southern Puna; 25°S–27°S) was characterized by the development of bimodal volcanism in the back-arc region (e.g., Kay et al., 1994; Petrinovic et al., 2006; Risse et al., 2008; Drew et al., 2009). Here, the basaltic andesite end member is represented by numerous cinder cones, lava flows, and maars grouped in small volcanic fields (Thorpe et al., 1984; Kay et al., 1994; Drew et al., 2009; Risse et al., 2008, 2013; Haag et al., 2019), and a rhyolitic end member is represented by lava domes, small phreatomagmatic volcanic centers, and collapse calderas, including the Cueros de Purulla, Cerro Chascon, and the Cerro Blanco volcanic complex, which is the focus here.

Local Geological Setting

The Cerro Blanco volcanic complex represents the most recent phase of the long-lived La Hoyada volcanic complex. The La Hoyada volcanic complex is formed by several Miocene–Pleistocene, SW-NE–aligned, andesitic-dacitic composite volcanoes that form the San Buenaventura range (Fig. 1D; Seggiaro et al., 2000; Montero López et al., 2010a; Bustos et al., 2019). The San Buenaventura range was developed above a complex upper-crustal basement (Fig. 1C). The immediate basement is a series of late Miocene (ca. 9–7 Ma), mainly rhyolitic ignimbrites, the source volcanoes of which have yet to be identified (Fig. 1C; Montero López et al., 2014, 2015). Beneath these, there are Precambrian–Lower Paleozoic metamorphic rocks of low to medium grade, Ordovician volcano-sedimentary sequences, Upper Paleozoic continental deposits, and Cenozoic deposits that infill the Paleogene foreland basins (Seggiaro et al., 2000).

The volcanic stratigraphy of the La Hoyada volcanic complex is divided into two main units (Fig. 1D; Bustos et al., 2019): (1) Lower La Hoyada (ca. 7–4.6 Ma), comprising andesitic-dacitic lava flows and domes characterized by a pervasive tectonic deformation; and (2) Upper La Hoyada (4.6–1.3 Ma), mainly represented by andesitic-dacitic effusive products and subordinate pyroclastic and epiclastic deposits that form part of at least four volcanic edifices (stratovolcanoes and domes). The most recent stage of the Upper La Hoyada volcanic complex is the Cerro Blanco volcanic complex, a nested set of Upper Pleistocene to Holocene calderas.

Cerro Blanco Volcanic Complex

The Cerro Blanco volcanic complex (Fig. 2) represents a 15-km-wide, nested caldera cluster formed by several scarps with different topographical expressions and degrees of preservation, along with associated domes and pyroclastic deposits (Montero López et al., 2010a; Báez et al., 2015, 2017). It is the most recent stage of the La Hoyada volcanic complex and is built on top of Upper La Hoyada volcanic complex. In this sense, it is a Krakatau- or Crater Lake–type caldera complex, resulting from the collapse of a long-lived composite volcano (e.g., Williams and McBirney, 1979), although it is multicyclic. The components of the Cerro Blanco volcanic complex include the well-defined Cerro Blanco and Robledo calderas (de Silva and Francis, 1991; Seggiaro et al., 2000), the poorly expressed Pie de San Buenaventura caldera (Montero López et al., 2010a), and the large El Niño scarp (Arnosio et al., 2005, 2008). The best-preserved structure in the Cerro Blanco volcanic complex is the subcircular Cerro Blanco caldera, which is ~4 km wide with fresh walls that reach 300 m in height. All erupted products are rhyolitic/rhyodacitic in composition and middle Pleistocene–Holocene in age (Montero López et al., 2010a; Báez et al., 2015, 2020a, 2020b; Fernández-Turiel et al., 2019). The Cerro Blanco volcanic complex hosts an important geothermal field (Viramonte et al., 2005; Chiodi et al., 2019) that has been deflating at a linear subsidence rate of –1.0 cm/yr since 1995 (Henderson and Pritchard, 2013).

The proximal and medial Cerro Blanco volcanic complex stratigraphy consists of two main ignimbrite units (Fig. 2B) separated by a major unconformity that represents a significant period of quiescence between the two eruptions (Báez et al., 2015, and references therein). The older is the late Pleistocene (73.24 ± 23.2 ka; Báez et al., 2015) Campo de la Piedra Pómez ignimbrite, also known as "cycle 1" in Montero López et al. (2010a). This is related to the first large caldera collapse in the evolution of the Cerro Blanco volcanic complex, now expressed as the Pie de San Buenavenutra and El Niño scarps (Báez et al., 2020b). The Campo Piedra Pomez ignimbrite eruption started with a Plinian fallout phase that initiated caldera collapse and a large volume of sustained pyroclastic density currents (PDCs; a.k.a. pyroclastic flows, ash flows)

generated by low pyroclastic fountains (boiling over) along the ring faults (Báez, 2015; Báez et al., 2020b). The PDCs were high-particle-concentration (dense), low-velocity currents, with limited capability to surmount even low topography (Báez et al., 2015, 2020b). The minimum volume is estimated to be at least 10 km^3 (magma equivalent), translating to a volcanic explosivity index (VEI) >6 (Báez et al., 2015, 2020b).

The 4.2 ka Cerro Blanco ignimbrite and associated deposits were defined by Báez et al. (2015), but they had previously been termed "cycle 2" in Montero López et al. (2010a). The Cerro Blanco ignimbrite is a nonwelded, pumice-rich, white to buff ignimbrite that crops out radial to the Cerro Blanco caldera, covering an area of ~527 km^2 and reaching a maximum runout distance of 40 km from the caldera border (Fig. 1D). The juvenile clasts in the Cerro Blanco ignimbrite are predominantly glassy, white rhyolitic pumice. Accessory and accidental lithic clasts are mainly Neoproterozoic–early Paleozoic plutonic-metamorphic rocks and Miocene–Pleistocene andesitic/dacitic lavas. Occasional cognate clasts of rhyolitic lavas are present. A total deposit volume of 15.2 km^3 (without lithics) and a dense rock equivalent or magma volume of 8.3 km^3 have been estimated (Báez et al., 2015, 2020a). Besides the pyroclastic deposits related to the paroxysmal stage of the 4.2 ka Cerro Blanco caldera-forming eruption, many studies described pre- and post–Cerro Blanco ignimbrite minor activity. This activity was in part effusive, represented by precaldera block-and-ash-flow deposits cropping out in the northwest caldera wall (Báez et al., 2015, and references therein). In addition, pre–Cerro Blanco ignimbrite explosive activity is recorded by a series of fallout deposits interbedded with peat that underlie the Cerro Blanco ignimbrite 12 km southward of the caldera, and these have been dated between 8830 ± 60 cal yr B.P. and 5480 ± 40 cal yr B.P. (Montero López et al., 2009, 2010a).

The final stage (post–Cerro Blanco ignimbrite) is referred to as postcaldera activity and was concentrated along a lineament trending 60° (NE). This phase was mainly effusive and produced several lava domes and block-and-ash-flow deposits emplaced in the southwestern caldera border (Arnosio et al., 2005; Montero López et al., 2009, 2010a). The mechanisms of lava-dome growth and destruction have been addressed by Báez et al. (2017). The postcaldera activity also included phreatomagmatic-phreatic small explosions (Montero López et al., 2010a; Báez et al., 2017a; Chiodi et al., 2019).

Petrochemical Framework—Previous Reconnaissance Work

Series of reconnaissance studies have been conducted that established the mineral assemblage of Cerro Blanco volcanic complex. The juvenile material is composed of Na-plagioclase, sanidine, and quartz, with minor biotite, oxides, orthopyroxene, and clinopyroxene immersed in a vesiculated holohyaline glass (Arnosio et al., 2005; Montero López et al., 2010a; Báez et al., 2015; Bardelli et al., 2020). Distinguishing features of the different Cerro Blanco volcanic complex rhyolites are their crystal contents. Samples from Campo Piedra Pomez ignimbrite are relatively crystal-rich (5%–20%) rhyolites, whereas the Cerro Blanco ignimbrite pumices are crystal-poor rocks (<5%). A suite of darker pumices and selvages is also found in the Campo Piedra Pomez ignimbrite, and it has andesitic compositions (55.5–57.2% SiO_2; Bardelli et al., 2020). Associated petrochemical data are at a reconnaissance level (Arnosio et al., 2005; Viramonte et al., 2005; Montero López et al., 2010a; Báez et al., 2015), but the evidence for recharge into the Campo Piedra Pomez ignimbrite magma reservoir has been presented in detail by Bardelli et al. (2020). On the basis of their petrographic and microanalytical study of mafic enclaves and andesitic bands within the rhyolitic pumice, Bardelli et al. (2020) suggested that parental andesitic to basaltic andesitic magmas ponded, mixed, and mingled with rhyolitic magma at a depth of 10 km (2.7 kbar based on two-pyroxene thermobarometry).

Cerro Blanco volcanic complex rhyolites have been classified as calc-alkaline (Fig. 3) and form two distinctive groups (Arnosio et al., 2005; Montero López et al., 2010a): (1) The Campo Piedra Pomez ignimbrite is dominantly low-silica rhyolite (70–75 wt% SiO_2), with high Sr, Ba, and Zr contents, low Rb contents, and a weak negative Eu anomaly. (2) The Cerro Blanco ignimbrite and post–Cerro Blanco ignimbrite eruptives are high-silica rhyolites (75–77 wt% SiO_2) with high Rb content, strong negative Eu anomaly, and low Sr, Ba, and Zr contents (Fig. 4). Preliminary data from melt inclusions in quartz and sanidine phenocrysts indicate pre-eruptive H_2O contents ranging from 1.1 to 8.6 wt% (Roberge et al., 2018). Magmatic temperatures of around 760–820 °C and 600–750 °C were estimated based on Fe-Ti–oxide equilibria for the Campo Piedra Pomez ignimbrite and Cerro Blanco ignimbrite, respectively (Báez, 2015; Fernández-Turiel et al., 2019). Arnosio et al. (2008) qualitatively interpreted these characteristics as the result of a cogenetic magmatic system that initiated deep (below the depth of plagioclase stability) during formation of the Campo Piedra Pomez ignimbrite magma but then ascended to shallow levels to evolve and erupt the younger group of magmas.

Siebel et al. (2001) and Schnurr et al. (2007) published data for two samples of Campo Piedra Pomez ignimbrite pumice and included them in their "arc-related" group of southern Puna ignimbrites based on the trace-element and isotopic character (one sample). They proposed that the entire Cerro Blanco volcanic complex likely involved significant assimilation of basement lithologies and represents the surface manifestation of a small arc-related plutonic complex that was built episodically. These authors also published data for rhyolites erupted from centers near the Cerro Blanco volcanic complex, the Cerro Chascon and Cueros de Purulla, which we refer to herein as "other rhyolites" in any comparisons with the Cerro Blanco volcanic complex.

SAMPLING AND METHODS

In total, 18 new samples of pumices and juvenile clasts were analyzed from the Campo Piedra Pomez ignimbrite (6), Cerro Blanco ignimbrite (6), and postcaldera (6) stages of the Cerro Blanco volcanic complex (Fig. 2). These sample sites were chosen to maximize sampling of the main deposits in the stratigraphy

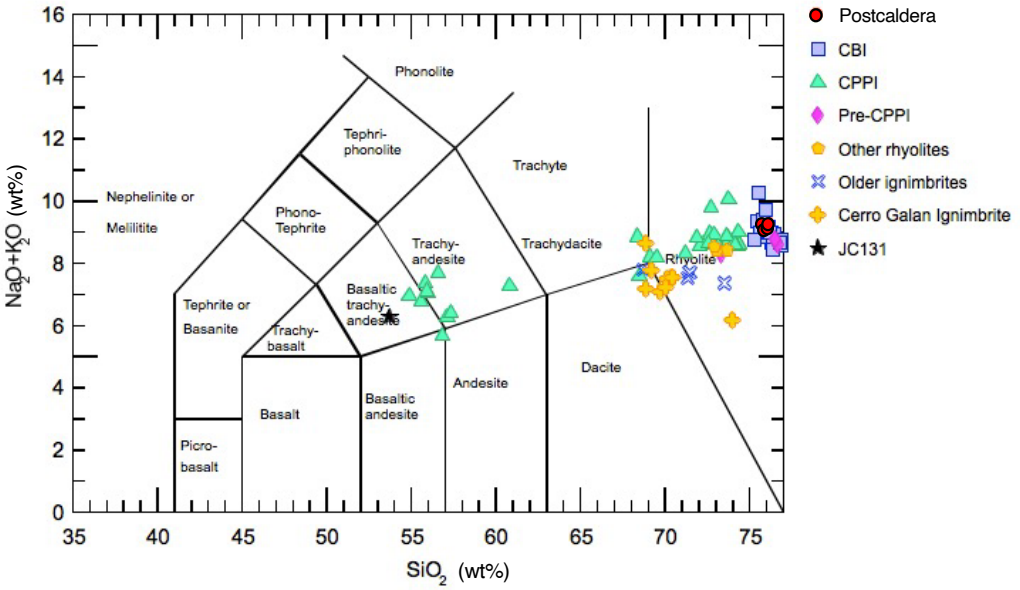

Figure 3. Total alkalis vs. SiO_2 diagram after Le Bas et al. (1986) and Le Maitre (1984). Nomenclature and abbreviations of the Cerro Blanco volcanic complex eruptive groups follow Figure 2. Also shown are other rhyolites from neighborhood centers Cueros de Purulla and Cerro Chascon, the 2.0 Ma Cerro Galan ignimbrite (CBI), other pre–La Hoyada ignimbrites (Aguada Alumbrera and Rosada), and JC131, a basaltic trachyandesite from the Antofagasta de la Sierra volcanic field used by Francis et al. (1989) as a potential proxy for the mafic input into the upper-crustal magma system of Cerro Galan, ~100 km northeast of the La Hoyada volcanic complex. See text for further discussion. CPPI—Campo Piedra Pomez ignimbrite.

and to fill in gaps in the existing database of Arnosio et al. (2005) and Báez et al. (2015) compiled in the supplemental material (Supplemental Table S2[1]).

$^{40}Ar/^{39}Ar$ Dating

Sanidine crystals from a single sample of pumice from the Campo Piedra Pomez ignimbrite (CB6) were separated and purified using the standard procedures in the Ar-Ar Geochronology Laboratory at Oregon State University. Handpicked sanidine crystals were then packaged and irradiated at the TRIGA nuclear reactor at Oregon State University. These crystals were then analyzed as single-crystal total fusions on the ARGUS-VI multicollector mass spectrometer. A weighted mean age was calculated following the ideogram approach (population density plots) using the ArArCALC v2.7.0 software (Koppers, 2002), and ages are reported in Supplemental Table S1. Full sample preparation, analytical methods, and calculation procedures are given in Supplemental File S1, and the full data set is given in Supplemental Table S1.

[1]Supplemental Material. Methodology, calculations, and data analysis. Please visit https://doi.org/10.1130/GEOS.S.16934566 to access the supplemental material, and contact editing@geosociety.org with any questions.

Whole-Rock Major- and Trace-Element Analyses

New whole-rock major and trace elements of 14 samples collected in 2007 were analyzed by X-ray fluorescence (XRF) at the Laboratorio Universitario de Geoquimica Isotopica (LUGIS) at Universidad Nacional Autonoma Mexico using a Siemens SRS3000 sequential spectrometer, with an end window rhenium (Rh) target. The calibration curves were built using 35 international reference standards (for more details on the procedure, see Lozano and Bernal, 2005). Estimated analytical errors are ~1% and ~4% for major and trace elements, respectively.

Additionally, four further samples along with duplicates of some of the 2007 samples were analyzed at the Washington State University GeoAnalytical Laboratory. Whole-rock major and trace elements were measured by XRF techniques using a ThermoARL system. Trace elements, including rare earth elements (REEs), were measured via inductively coupled plasma–mass spectrometry (ICP-MS) using an Agilent 7700 quadrupole mass spectrometer. Analytical methods are described in Johnson et al. (1999). Duplicates of the 2007 samples analyzed in the second batch showed good agreement with the first batch. Representative analyses are given in Table 1, and the full data set is available in the supplemental data (Supplemental Table S2).

Data for a further 74 samples from literature (Siebel et al., 2001; Arnosio et al., 2005; Báez et al., 2015; Montero López et al., 2010a; Bardelli et al., 2020)

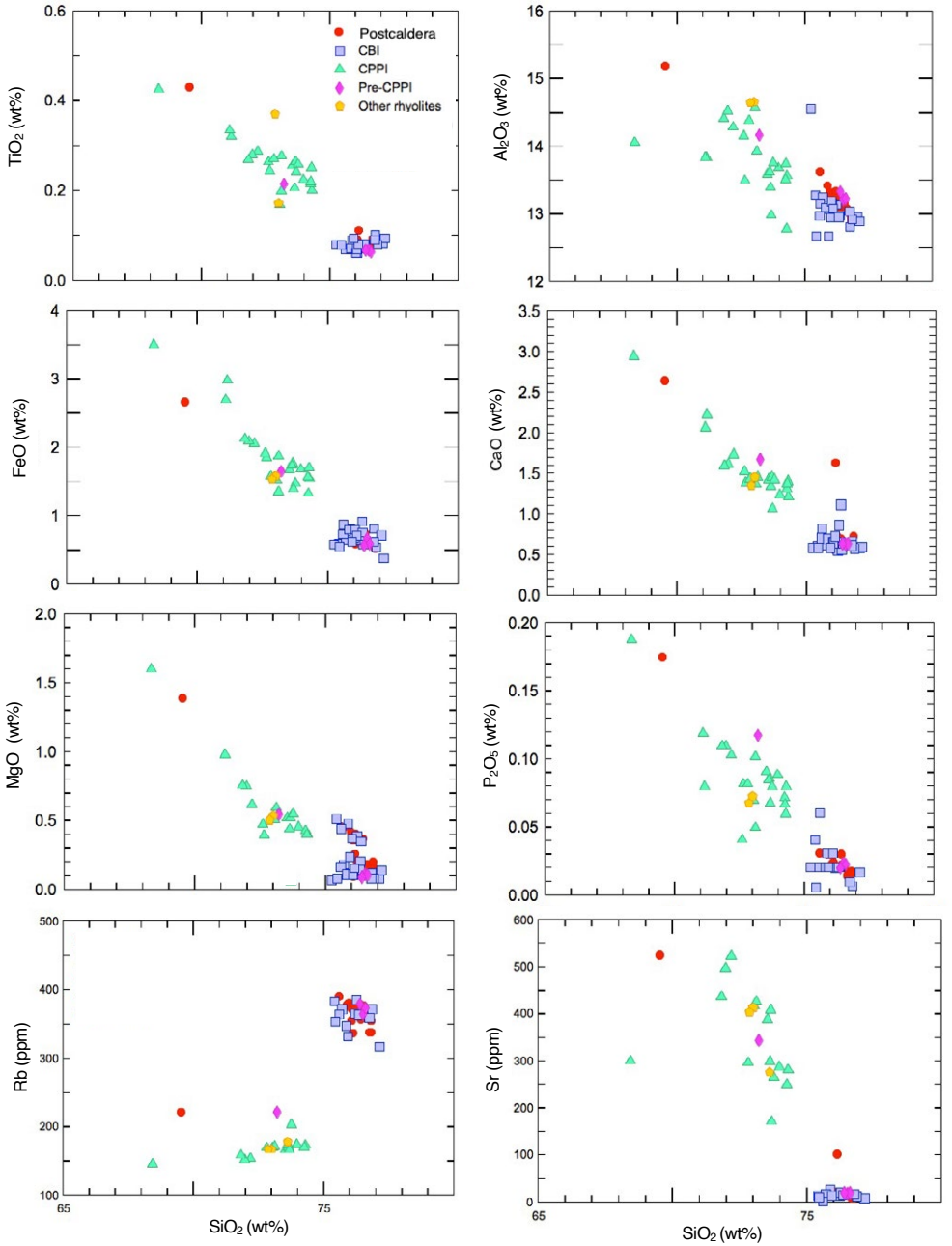

Figure 4. Harker diagrams for selected major elements, Rb, and Sr vs. SiO_2 for the siliceous compositions in the Cerro Blanco volcanic complex suite. Shown here are the data for samples with SiO_2 >67% only. Analyses were normalized on a 100% anhydrous basis. All major elements, except for Na_2O and MnO, are compatible. CBI—Cerro Galan ignimbrite; CPPI—Campo Piedra Pomez ignimbrite.

TABLE 1. SELECTED NEW BULK-ROCK MAJOR- AND TRACE-ELEMENT ANALYSES OF CERRO BLANCO VOLCANIC COMPLEX LITHOLOGIES

Unit:	Campo de la Piedra Pomez				Cerro Blanco ignimbrite			Postcaldera (PC)		
Sample:	CPP16001	CB07-11	CB07-03	CB11-01	Purulla 2018	CB07-10	CPP18001	CB07-13	CB07-12A	CB07-06
Material:	Basal pumice fall	Ignimbrite	Ignimbrite	Ignimbrite	Ignimbrite	Ignimbrite	Ignimbrite	PDC	BAF	Lava dome
SiO_2	73.67	73.74	72.79	74.23	76.83	75.43	76.73	76.14	76.83	76.75
TiO_2	0.24	0.26	0.27	0.22	0.08	0.08	0.09	0.11	0.09	0.09
Al_2O_3	12.99	13.76	14.39	13.75	12.93	12.68	13.05	13.14	12.93	12.99
FeO	1.40	1.48	1.58	1.33	0.54	0.55	0.62	0.73	0.51	0.57
MgO	0.06	0.55	0.06	0.05	0.08	0.08	0.08	0.26	0.16	0.14
MnO	0.40	0.05	0.42	0.34	0.13	0.26	0.09	0.08	0.07	0.07
CaO	1.07	1.43	1.44	1.38	0.58	0.59	0.62	0.63	0.59	0.62
Na_2O	4.91	4.94	3.95	3.68	4.20	5.71	4.09	4.26	4.74	4.70
K_2O	5.18	3.71	5.01	4.94	4.62	4.62	4.62	4.63	4.05	4.06
P_2O_5	0.07	0.08	0.08	0.07	0.01	0.01	0.01	0.02	0.02	0.02
Total	100.00	100.00	100.00	100.00	100.00	100.00	100.00	100.00	100.00	100.00
Ba	486	599	826	626	11	10	32	32	24	30
Rb	167	204	170	171	372	354	360	337	338	338
Sr	172	267	297	251	12	12	18	101	10	9
Zr	156	185	192	155	64	61	66	86	76	74
Y	16	42	16	15	20	18	19	45	44	41
Nb	27	26	29	27	51	48	48	46	48	50
Ta	1.6	2.4	2.4	2.4	5.0	4.6	4.6	4.3	4.5	4.5
Hf	3.0	5.1	5.3	4.5	3.6	3.4	3.4	3.4	3.4	3.4
Cs	11.3	7.2	6.8	7.1	30.6	28.8	29.0	29.0	29.0	29.0
Pb	22.4	22.0	21.4	18.9	35.5	32.3	33.2	35.0	35.0	37.0
Th	24.5	24.5	24.6	25.3	31.5	29.0	30.5	29.0	31.5	30.5
U	6.9	7.1	7.2	7.3	22.6	22.6	22.8	22.8	22.8	22.7
La	40.7	56.4	59.8	55.4	18.6	18.0	18.2	18.7	18.6	23.5
Ce	70.3	101.5	104.7	96.9	39.4	37.5	37.9	37.2	37.2	47.3
Pr	7.0	10.2	10.5	9.7	4.4	4.2	4.3	4.2	4.3	5.6
Nd	22.2	32.4	33.7	31.0	15.0	14.0	14.2	14.7	14.9	19.3
Sm	3.5	5.1	5.2	5.0	3.2	3.0	3.0	3.1	3.0	3.8
Eu	0.6	1.0	1.1	1.0	0.2	0.2	0.2	0.2	0.2	0.2
Gd	2.4	3.6	3.7	3.4	2.7	2.5	2.6	2.8	2.8	3.4
Tb	0.4	0.5	0.6	0.5	0.5	0.4	0.4	0.5	0.5	0.6
Dy	2.0	3.1	3.1	3.0	3.0	2.8	2.8	2.7	2.8	3.7
Ho	0.4	0.6	0.6	0.6	0.6	0.6	0.6	0.6	0.6	0.7
Er	1.1	1.6	1.6	1.6	2.0	1.7	1.8	1.9	1.9	2.4
Tm	0.2	0.2	0.2	0.2	0.3	0.3	0.3	0.3	0.3	0.3
Yb	1.0	1.5	1.5	1.5	2.3	2.1	2.1	2.3	2.5	3.0
Lu	0.2	0.2	0.2	0.2	0.4	0.4	0.4	0.4	0.4	0.4

Note: All analyses are juvenile material—pumice, poorly expanded rhyolite, and lava. PDC—pyroclastic density current; BAF—block-and-ash flow. Major oxides are given in wt%, and trace elements are given in ppm.

and unpublished sources were compiled and used in our analysis. The full compiled data sets are given in the supplemental data (Supplemental Tables S2 and S2b). All major-element data presented in figures and tables herein have been recalculated to 100% on an anhydrous basis; the unnormalized data are in Supplemental Table S2b.

Whole-Rock Radiogenic Isotope Analyses

Whole-rock powders from eight representative samples were analyzed for $^{87}Sr/^{86}Sr$, $^{143}Nd/^{144}Nd$, $^{206}Pb/^{204}Pb$, $^{207}Pb/^{204}Pb$, and $^{208}Pb/^{204}Pb$ at New Mexico State University using thermal ionization mass spectrometry (TIMS). Samples were digested by dissolving 200–400 mg of rock powder using hydrofluoric, nitric, and hydrochloric acids. For Sr isotopes, Sr was purified using cation exchange resin and 2.5 *N* HCl. Sr was then loaded onto pre-outgassed and clean rhenium filaments with phosphoric acid and tantalum oxide. Sr isotopes were analyzed using TIMS and five Faraday collectors in dynamic mode and ^{88}Sr = 3.0V. Sr isotopes were normalized to $^{86}Sr/^{88}Sr$ = 0119. For Nd isotopes, REEs were purified using cation exchange resin and 6.0 *N* HCl. Nd was then separated/purified from the remaining REEs using HDEHP resin and 0.25 *N* HCl. Nd was loaded onto pre-outgassed and clean rhenium triple filaments. Nd isotopes were analyzed using TIMS and five Faraday collectors in dynamic mode with ^{144}Nd = 0.5V. Nd isotopes were normalized to $^{146}Nd/^{144}Nd$ = 0.7219 and corrected for any Sm present during the analysis. For Pb isotopes, Pb was purified using anion exchange resin and 1.0 *N* HBr. Pb was dissolved in 1 mL of 2% HNO_3, and Tl was introduced into the sample to obtain a Pb/Tl ratio between 2 and 5 (Wolff and Ramos, 2003). Samples were analyzed using a ThermoScientific Neptune in static mode using five Faraday collectors. Pb isotope results were normalized to $^{203}Tl/^{205}Tl$ = 0.41892 and corrected for Hg during analysis. Reproducibility of $^{87}Sr/^{86}Sr$ and $^{143}Nd/^{144}Nd$ was within 0.000025 and 0.00003, respectively, based on analyses of standards. Data are presented in Table 2A. Additional details on the TIMS procedure can be found in Ramos (1992) and in the supplemental data (Supplemental Table S4).

Single-Crystal O Isotope Analyses

Handpicked quartz crystals from representative samples were analyzed at the University of Oregon for oxygen isotope compositions (Bindeman, 2008, and references therein). CO_2-laser fluorination and a 35 W laser were used. Individual and bulk mineral grains ranging in weight between 0.6 and 2 mg were reacted in the presence of purified BrF_5 reagent to liberate oxygen. The gases generated in the laser chamber were purified through a series of cryogenic traps held at liquid nitrogen temperature, and a mercury diffusion pump was used to eliminate traces of fluorine gas. Oxygen was converted to CO_2 gas by a small platinum-graphite converter, the yield was measured, and then CO_2 gas was analyzed on a MAT 253 mass spectrometer. Three to seven standards were analyzed together with the unknowns during each analytical session. San Carlos olivine ($\delta^{18}O$ = +5.35‰) and Gore Mountain garnet ($\delta^{18}O$ = +5.75‰) were used as standards. Day-to-day $\delta^{18}O$ variability (= $\delta^{18}O$[Standard] – $\delta^{18}O$[Measured standard]) ranged from 0.1‰ to 0.25‰, and these values were added to the unknowns to correct for day-to-day standard offset. Values are reported on the standard mean ocean water (SMOW) scale and are reported as $\delta^{18}O$ (‰). Data are presented in Table 2B. Additional details of the analytical procedure are given in the supplemental files (Supplemental Table S5). The precision on standards and duplicates of quartz samples was <0.1‰.

Matrix Glass Major- and Trace-Element Analyses

Major-element compositions of matrix glasses were obtained by electron microprobe analysis (EPMA) using a Cameca SX-100 electron microprobe at Oregon State University with a 15 kV accelerating voltage, 30 nA beam current, and a beam diameter of 5 mm following the practice explained in Tepley et al. (2013). Both glass and mineral standards were used. The analyses were performed on polished thin sections of handpicked pumiceous glass fragments that were mounted in epoxy. An average matrix glass composition for each eruptive unit was calculated for 10 major-element oxides (SiO_2,

TABLE 2A. THERMAL IONIZATION MASS SPECTROMETRY ANALYSES OF RADIOGENIC ISOTOPES OF CERRO BLANCO VOLCANIC COMPLEX LITHOLOGIES

Sample	Unit	$^{87}Sr/^{86}Sr$	Error	$^{143}Nd/^{144}Nd$	Error	$^{206}Pb/^{204}Pb$	Error	$^{207}Pb/^{204}Pb$	Error	$^{208}Pb/^{204}Pb$	Error
DOMO 01	Postcaldera	0.706799	0.000007	0.512516	0.000009	18.958	0.001	15.651	0.001	39.001	0.002
CBV 02	Postcaldera	0.706792	0.000010	0.512505	0.000012	18.963	0.001	15.645	0.001	39.001	0.002
CB 20-D	CBI	0.706958	0.000008	0.512528	0.000010	18.960	0.001	15.645	0.001	39.001	0.002
Cpomez 01	CBI	0.706615	0.000008	0.512524	0.000011	18.965	0.001	15.646	0.001	39.001	0.002
CB 35	CBI	0.707407	0.000008	0.512505	0.000009	18.963	0.001	15.646	0.001	39.001	0.002
CBV 12A	CPPI	0.706626	0.000011	0.512531	0.000010	18.964	0.001	15.645	0.002	39.002	0.004
CB6	CPPI	0.706628	0.000011	0.512534	0.000016	18.954	0.001	15.642	0.001	39.003	0.004
CB44	Pre-CPP (SE)	0.706839	0.000008	0.512519	0.000010	18.964	0.001	15.643	0.001	39.001	0.002

Note: Analyses were completed at New Mexico State University. See text and Supplemental Information (text footnote 1) for analytical details and standards. CBI—Cerro Blanco ignimbrite; CPPI—Campo Piedra Pomez ignimbrite; pre-CPP—pre–Campo Piedra Pomez.

TABLE 2B. O ISOTOPE ANALYSES OF CERRO BLANCO VOLCANIC COMPLEX LITHOLOGIES

Sample	Unit	Material	$\delta^{18}O$
CB07-12B	Postcaldera	Qz, single cr	8.35
CB07-14	Postcaldera	Qz, single cr	8.56
CB07-13	Postcaldera	Qz, 2 cr	8.55
CB07-08	Postcaldera	Qz, single cr	8.47
CB07-06	Postcaldera	Qz, single cr	8.20
CB07-15	CBI	Qz, single cr	8.71
CB07-05	CBI	Qz, single cr	8.68
CB07-10	CBI	Qz, single cr	8.40
CB07-02B	CPPI (basal fall)	Qz, 2 cr	7.63
CB07-01	CPPI	Sanidine	6.7
CB07-03	CPPI	Qz, single cr	8.34
CB07-11	CPPI	Qz, 2 cr	8.36
CB-6	CPPI	Qz, 2 cr	8.12

Note: Analyses were conducted at the University of Oregon. See text and Supplemental Information (text footnote 1) for analytical details and standard data. CBI—Cerro Blanco ignimbrite; CPPI—Campo Piedra Pomez ignimbrite; Qz—quartz; single cr—single crystal; 2 cr—two crystals.

Al_2O_3, K_2O, CaO, MnO, FeO [total Fe], Na_2O, MgO, TiO_2, P_2O_5; see Supplemental Table S3). Replicate analyses showed little variability (<1% for SiO_2 and Al_2O_3; <5% for K_2O, CaO, MnO, FeO, Na_2O, MgO, and TiO_2). Average analyses are presented in Table 3, and the full data set is presented in the supplemental data (Supplemental Table S3). To correct for alkali migration during analysis (Nielsen and Sigurdsson, 1981; Lowenstern, 1995), we used the zero-time intercept function on Na, K, and Si and Al (these last two tend to rise with time, not decrease). This is discussed further in the supplemental materials (Supplemental Table S3b) along with a discussion of our reproducibility for secondary standards.

Trace-element concentrations of matrix glasses were measured by laser-ablation (LA) ICP-MS at Oregon State University. See Kent et al. (2004) for details on the technique. Abundances of individual trace elements were calculated relative to the U.S. Geological Survey (USGS) glass standard BCR-2G, which was analyzed under identical conditions throughout the analytical session. Standard 29Si was used as an internal standard in conjunction with average SiO_2 contents measured by electron probe. BHVO-2G and ATHO-G glasses were used to monitor accuracy and precision, and results indicated that both these were within ±10% for all trace element analyzed. Although dependent upon elemental abundances in individual glass samples, external errors (see Kent et al., 2004) calculated from multiple analyses were typically ±5% for most elements (Rb, Sr, Y, Zr, Nb, Ba, La, Ce, Pr); ±10% for Hf and Nd; and ±15% for Sm, Eu, Gd, Dy, Er, and Yb (at 2σ). Average analyses are presented in Table 3, and the full data set is presented in supplemental data (Supplemental Table S3) along with a discussion of primary standards used and a discussion of our reproducibility for secondary standards.

RESULTS

For the purposes of this contribution, we eschew the cycle 1 and cycle 2 terminology of Montero López et al. (2010b) because we will show that the pre–Campo Piedra Pomez ignimbrite lithologies have geochemical characteristics that group them with Cerro Blanco ignimbrite and cycle 2, and this makes such a division geochemically confusing. Instead, we will refer to four stages: pre–Campo Piedra Pomez ignimbrite, Campo Piedra Pomez ignimbrite, Cerro Blanco ignimbrite, and postcaldera (post–Cerro Blanco ignimbrite) (Fig. 2).

Eruption Age

The 25 single sanidine crystal fusions yielded a range of new ages that define three different age populations based on age probability distributions (ideograms) within Ar-Ar calc (Koppers, 2002). These populations have weighted mean ages of 86.3 ± 8.2 ka (5 crystals), 65.3 ± 1.2 ka (13 crystals), and 54.6 ± 0.6 ka (7 crystals). The data and results of the statistical analysis are presented in Supplemental File S1 and Table S1. The weighted mean age of the youngest population is taken here as the new preferred age for the Campo Piedra Pomez ignimbrite eruption, as is common practice in single-crystal $^{40}Ar/^{39}Ar$ dating for over three decades (e.g., Deino and Potts, 1992). Although apparently ~20 k.y. younger than the previously reported age of 73.24 ± 23.2 ka, the two ages are actually concordant, but our new age is far more precise. This reflects the difference between more accurate and precise single-crystal fusions versus bulk aggregate crystal fusions, where the latter probably reflect a mixed age of the three different populations. We use the new 54.6 ± 0.6 ka age henceforth.

Petrography

All samples examined contained an assemblage of plagioclase, quartz, sanidine, biotite, and amphibole as the major mineral phases. Fe-Ti oxides and apatite were ubiquitous minor constituents. Our samples from the Campo Piedra Pomez ignimbrite were generally more crystal-rich (5%–20%, although the majority were less than 10%) than the Cerro Blanco ignimbrite samples. The dome lavas and pyroclastic derivatives were extremely crystal-rich with >35% phenocrysts (generally >2 mm) by volume. Some of the samples from the dome lavas had as high as 50% phenocrysts (up to 5 mm) with a notable increase in quartz (up to 30% of the assemblage in some samples). The groundmass in the dome lavas was feldspar microlite-rich glass, whereas the pumice from the Campo Piedra Pomez and Cerro Blanco ignimbrites had a hyalohaline groundmass. The Campo Piedra Pomez ignimbrite was characterized by higher plagioclase content than sanidine and quartz together. Some samples of the fall deposit of the Campo Piedra Pomez ignimbrite were relatively biotite- and amphibole-rich (1%–2%) samples compared to all other Cerro Blanco volcanic

TABLE 3. AVERAGES OF IN SITU MAJOR-ELEMENT (EPMA) AND TRACE-ELEMENT (LA-ICP-MS) MEASUREMENTS OF MATRIX GLASS FROM CERRO BLANCO VOLCANIC COMPLEX RHYOLITIC UNITS

Unit	CPPI				CBI		Postcaldera		
Sample:	CB07-03	CB07-02A (ave)	CB07-2B (ave)	CB07-11 (ave)	CB07-05 (ave)	CB07-10 (ave)	CB07-13 (ave)	CB07-12A (ave)	CB07-12B (ave)
Material:	Ignimbrite	CPPI basal fall	CPPI basal fall	Ignimbrite	Ignimbrite	Ignimbrite	PDC	BAF	BAF
SiO_2	76.32	76.73	76.94	76.82	76.88	76.69	77.17	76.47	76.55
TiO_2	0.14	0.10	0.09	0.14	0.08	0.07	0.08	0.08	0.08
Al_2O_3	13.13	13.11	12.86	13.03	13.38	13.26	13.41	13.14	13.20
FeO	0.20	0.55	0.61	0.80	0.47	0.48	0.48	0.48	0.48
MgO	0.07	0.06	0.06	0.10	0.05	0.06	0.05	0.04	0.04
MnO	0.02	0.03	0.06	0.06	0.10	0.09	0.08	0.09	0.08
CaO	0.76	0.71	0.69	0.76	0.53	0.52	0.54	0.51	0.51
Na_2O	3.99	2.87	2.67	2.93	3.88	4.27	3.55	4.63	4.54
K_2O	5.34	5.83	6.01	5.34	4.63	4.54	4.64	4.55	4.51
P_2O_5	0.02	0.00	0.00	0.02	0.01	0.01	0.00	0.01	0.00
Total	100.00	100.00	100.00	100.00	100.00	100.00	100.00	100.00	100.00
Ba	370	50	46	388	3	3	7	2	5
Rb	216	280	313	200	466	483	422	424	470
Sr	103	430	68	109	4	4	32	4	5
Zr	147	127	121	153	87	96	48	81	73
Y	26	6	6	27	32	35	18	28	26
Nb	36	29	27	36	75	74	61	67	72
Hf	4	6	6	5	6	6	3	5	4
V	4	9	5	4	1	1	5	1	3
Pb	32	50	32	36	49	48	38	44	44
La	59	38	34	63	19	19	14	17	14
Ce	93	37	35	95	40	36	33	36	36
Pr	9	3	3	10	5	5	4	4	4
Nd	29	9	7	35	18	17	13	17	14
Sm	5	1	1	6	4	4	3	3	3
Eu	1	0	0	1	0	0	0	0	0
Gd	5	1	1	5	4	4	2	4	3
Dy	4	1	1	4	5	5	3	4	4
Er	2	1	1	2	3	3	2	3	2
Yb	2	1	1	2	4	4	2	3	3
Eu/Eu*	0.45	0.63	0.61	0.45	0.12	0.14	0.21	0.14	0.13
Dy_N	15.97	2.34	2.83	17.04	18.77	18.87	10.75	15.86	14.25
La_N	249.71	158.73	144.26	267.87	79.91	78.83	57.00	70.17	60.71
Yb_N	7.19	4.18	4.52	9.61	16.38	16.13	8.74	12.58	10.97
Dy/Dy*	0.75	0.18	0.22	0.64	0.70	0.72	0.69	0.74	0.77

Note: EPMA—electron probe microanalysis; LA-ICP-MS—laser ablation–inductively coupled plasma–mass spectrometry; CBI—Cerro Blanco ignimbrite; CPPI—Campo Piedra Pomez ignimbrite; ave—average; PDC—pyroclastic density current; BAF—block-and-ash flow. Major oxides are given in wt%, and trace elements are given in ppm.

complex samples. Samples of the younger Cerro Blanco ignimbrite were characterized by less than 5% plagioclase, sanidine, and quartz, with occasional (<<1%) biotite and amphibole. Fe-Ti oxides and apatite were ubiquitous minor constituents again (rare in thin section, but common in mineral separates). All the postcaldera samples had a mineral assemblage of plagioclase, quartz, sanidine, biotite, and amphibole with accessory Fe-Ti oxides and apatite. Zircon, allanite, and some titanite were found in mineral separates.

Whole-Rock Geochemistry: Major and Trace Elements

All Cerro Blanco volcanic complex rocks were high-K, calc-alkaline in composition and represent a bimodal suite of rhyolite and trachyandesite compositions (Fig. 3). Whole-rock silica contents from Cerro Blanco ignimbrite and post–Cerro Blanco ignimbrite, along with some of the pre–Campo Piedra Pomez ignimbrite, clustered together between 75.2 and 77.1 wt% SiO_2 (Fig. 3),

which make them among the most evolved ignimbrites found in the southern Puna and Central Andes as a whole. On the other hand, Campo Piedra Pomez ignimbrite whole-rock silica contents were lower than all other samples from the Cerro Blanco volcanic complex. The felsic pumices ranged between 68.30 and 74.28 wt% SiO_2. The trachyandesites within the Campo Piedra Pomez ignimbrite were the dark and banded pumices discussed in detail by Bardelli et al. (2020), which had a mafic composition at 54% SiO_2. Hereafter, we will focus on the 74–78% SiO_2 end of the spectrum because compositions <74% SiO_2 are likely to be mixed between the various andesite and rhyolites of the Campo Piedra Pomez ignimbrite and are rare compared to the rest of the suite.

Except for the K_2O and Na_2O contents (Fig. 3), negative correlations were observed for all the other major oxides on Harker diagrams (Fig. 4). Interestingly, there was no correlation with crystal content in the most siliceous compositions; the postcaldera domes, which were extremely porphyritic with over 50% phenocrysts, were the most evolved in terms of the major elements; these samples were also those that contained a higher modal abundance (proportion of the rock) of quartz. Another notable observation is that most of the pre–Campo Piedra Pomez ignimbrite samples except for one plotted with the Cerro Blanco ignimbrite and postcaldera groups. Two groups of Cerro Blanco ignimbrite and postcaldera dome samples could be defined by MgO and Na_2O.

The differentiation and groupings of the Cerro Blanco volcanic complex rhyolites were even clearer in trace element diagrams (Figs. 5 and 6). The comprehensive data set we compiled in this study confirmed previous reconnaissance work that showed that the Campo Piedra Pomez ignimbrite is defined by lower Cs, Rb, U, Ta, Nb, and the heavy (H) REEsYb and Lu, and higher Ba, Sr, Zr, and the light (L) to middle (M) REEs compared to the rest of the rhyolites. The distinction is particularly marked in key ratios, where the Campo Piedra Pomez ignimbrite group had low Rb/Sr (<1) and U/Th (0.3), and higher La/Yb (35–40), Sr/Y (7–22), and Sr/Yb (180–350) compared to Rb/Sr from 15 to 40, U/Th from 0.7 to 0.98, La/Yb from 9 to 10, Sr/Y from 1 to 2, and Sr/Yb from 8 to 12 in the rest of the suite. The high La/Yb of the Campo Piedra Pomez ignimbrite group was accompanied with a significantly less pronounced Eu anomaly (calculated using the geometric mean method), where Eu/Eu* was 0.65–0.79, compared to 0.15–0.33 for the rest.

One pre–Campo Piedra Pomez ignimbrite sample and one postcaldera dome, as well as the nearby rhyolites from Cueros de Purulla (other rhyolites), showed some affinity with the Campo Piedra Pomez ignimbrite (Figs. 4 and 6). The two groups of Cerro Blanco ignimbrite/postcaldera compositions that appeared to be differentiated by MgO and Na_2O had no complement in the trace elements, so we refer to these as one group henceforth.

Radiogenic Isotopes

The radiogenic isotope compositions of Cerro Blanco volcanic complex rhyolites defined a rather limited range (Fig. 7). All data discussed are presented as measured and were not age-corrected. The $^{86}Sr/^{87}Sr$ ranged from

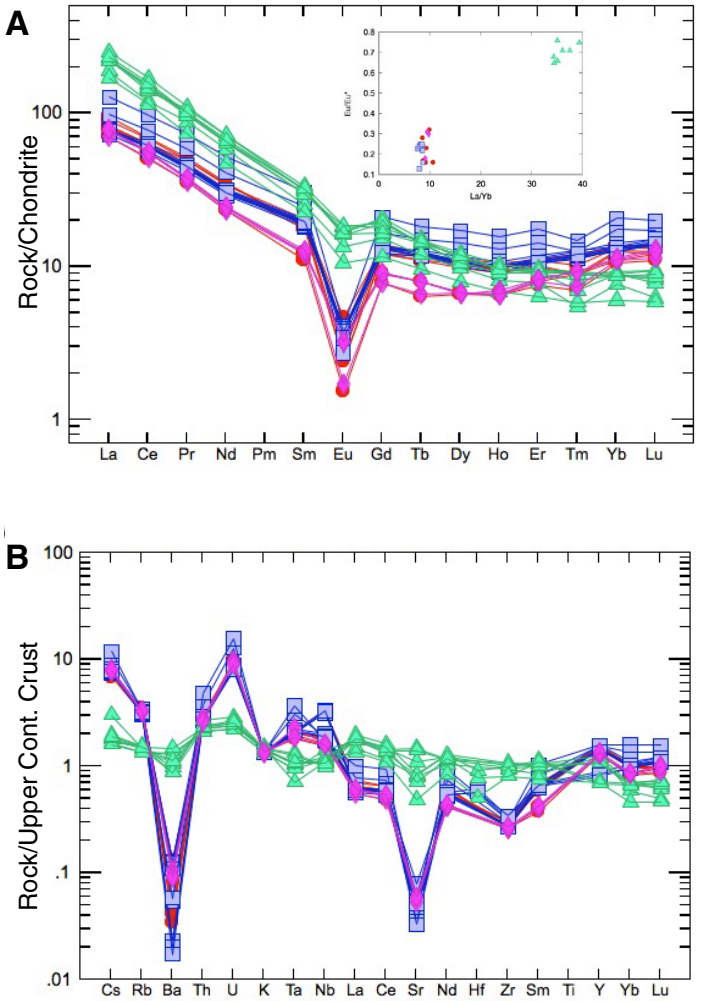

Figure 5. Multi-element diagrams for Campo Piedra Pomez ignimbrite (CPPI) and Cerro Blanco ignimbrite(CBI)/postcaldera bulk-rock compositions. Symbols are the same as in Figure 4. (A) Chondrite-normalized rare earth elements (REE; Sun and McDonough, 1989) showing the distinction between the Campo Piedra Pomez ignimbrite and Cerro Blanco ignimbrite/postcaldera compositions. The distinction is clear in the inset, which shows the low La/Yb vs. Eu/Eu* of the Cerro Blanco ignimbrite/postcaldera group compared with the Campo Piedra Pomez ignimbrite. (B) Upper continental crust–normalized spider diagram (Taylor and McLennan, 1985) revealing relative enrichments of Cs, Rb, U, Ta, Nb, Y, and heavy rare earth elements (HREEs) and depletions in Ba, Sr, light (L) REEs, Zr, and middle (M) REEs in the Cerro Blanco ignimbrite/postcaldera group relative to the Campo Piedra Pomez ignimbrite.

0.706615 to 0.707407, and $^{143}Nd/^{144}Nd$ had a range of 0.512505–0.512534. The Campo Piedra Pomez ignimbrite samples showed slightly lower $^{86}Sr/^{87}Sr$ than the Cerro Blanco ignimbrite/postcaldera samples. Our new data for $^{206}Pb/^{204}Pb$, $^{207}Pb/^{204}Pb$, and $^{208}Pb/^{204}Pb$ defined a very tight cluster. Ranges for the three different ratios were 18.854–18.965, 15.642–15.651, and 39.001–39.003 respectively, with no correlation with stratigraphy.

All our data are consistent with previous data for small southern Puna ignimbrites published by Siebel et al. (2001) and Schnurr et al. (2007) (Fig. 7). We note that the single analysis for the Cueros de Purulla ("Other rhyolite" in Fig. 7) has slightly higher $^{87}Sr/^{86}Sr$ and complementary lower eNd value compared with the Cerro Blanco volcanic complex. It has similar Pb isotope ratios to our Cerro Blanco volcanic complex data.

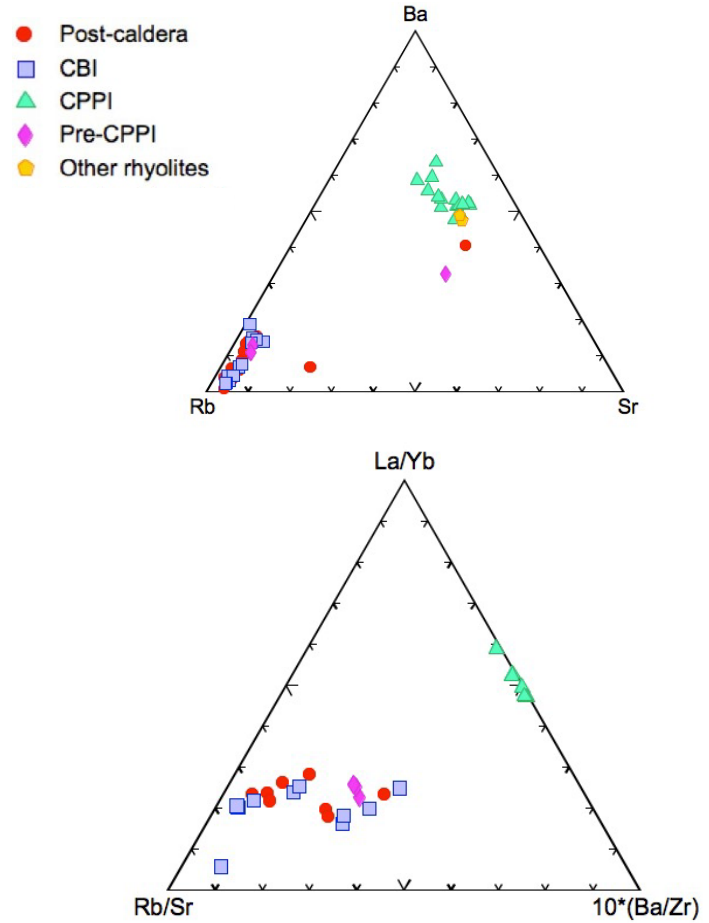

Figure 6. Trace-element discrimination diagrams for the Cerro Blanco volcanic complex rhyolites. Select ratios and groups of trace elements provide distinct geochemical fingerprints that facilitate correlations of detached and distal exposures of Cerro Blanco ignimbrite (CBI) and other tephras. Note the correlation of the other neighborhood rhyolites with the Campo Piedra Pomez ignimbrite (CPPI) in the upper figure. Not all trace elements are available in literature data. All data used are in ppm. gl—matrix glass.

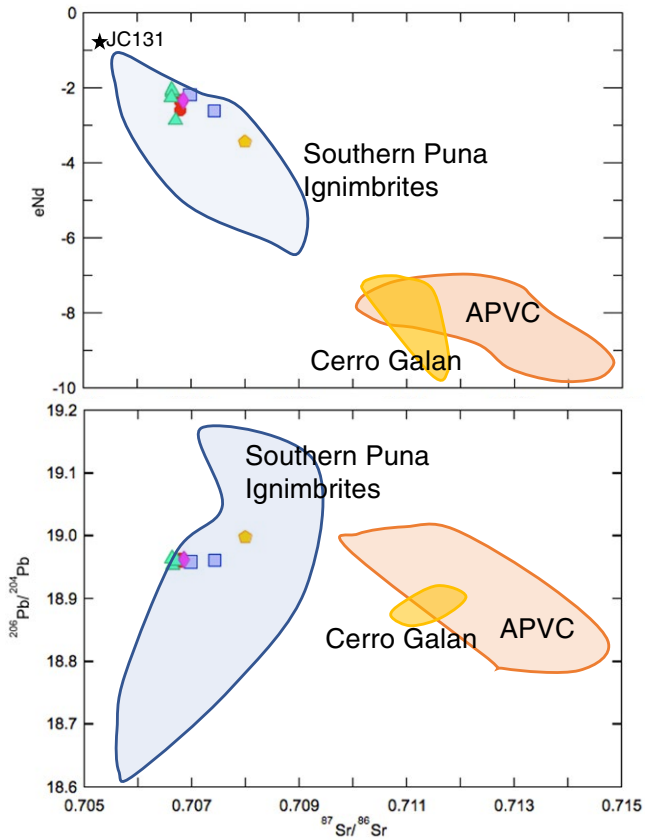

Figure 7. Radiogenic isotope covariation diagrams for available data for Cerro Blanco volcanic complex rhyolites in the context of regional and local siliceous volcanics. Data fields for southern Puna small ignimbrite are from Schnurr et al. (2007). Data for Altiplano-Puna Volcanic Complex (APVC) and Cerro Galan are from Folkes et al. (2013). Note that Cerro Blanco volcanic complex rhyolites define a tight group within the southern Puna small ignimbrites. Symbols are the same as in previous figures above. See text for further discussion.

Matrix Glass Geochemistry: In Situ Major and Trace Elements

In situ major-element compositions of matrix glass from the Cerro Blanco volcanic complex were all high-silica rhyolite in composition, with SiO_2 varying from ~76% to ~78 wt%, extending the range of the whole rock (Table 3; Fig. 8). The glass compositions of the Cerro Blanco ignimbrite and postcaldera samples were similar to slightly more evolved than the bulk rock. The matrix glasses in the Cerro Blanco ignimbrite extended to ~77% SiO_2, whereas the most siliceous matrix glass compositions came from the postcaldera domes, extending to almost 78%. The matrix glass compositions of Campo Piedra Pomez ignimbrite were up to 3 wt% SiO_2 more evolved than the corresponding bulk-rock host. The Campo Piedra Pomez ignimbrite matrix glass was distinguished from the Cerro Blanco ignimbrite and postcaldera glasses by higher CaO, TiO_2, and K_2O and lower Na_2O.

In situ trace elements of matrix glass from the Campo Piedra Pomez ignimbrite, Cerro Blanco ignimbrite, and post–Cerro Blanco ignimbrite lavas revealed that the Campo Piedra Pomez ignimbrite has significantly higher Zr, Sr, and LREE to MREE contents, and higher La/Yb and Eu/Eu* (smaller Eu anomaly) ratios (Fig. 9). The matrix glass from the other rhyolites had higher Rb, Nb, and HREE contents, and a higher Nb/Ta ratio. These differences are concordant with those seen in the bulk-rock data.

A feature of note is that matrix glass from samples of Campo Piedra Pomez ignimbrite Plinian fall (CB7-02A and -02B) had lower Ba and higher Sr than other matrix glass from the Campo Piedra Pomez ignimbrite. These values were accompanied by very distinct REE patterns with a deep concave-upward profile produced by a deep trough in the MREEs. This is clearly seen in the low Dy/Dy* <0.3 (calculated as in Davidson et al., 2012) compared with >0.5 for the rest of the suite. These glasses had the same distinct Eu/Eu* (geometric mean) and La/Yb ratios as the Campo Piedra Pomez ignimbrite; however, we note that Eu values were extremely depleted, indicating that both Eu^{2+} and Eu^{3+} have been significantly depleted.

O Isotope Determinations

O isotopes in quartz from pumices representing the siliceous eruptions at the Cerro Blanco volcanic complex defined a coherent group (Table 2B). As a suite of rhyolites, the range of $\delta^{18}O$ in quartz was from +8.12‰ to +8.71‰, with one sample (CB07–02B Campo Piedra Pomez ignimbrite Plinian fall) showing a significantly lower value of +7.63‰. Although there was significant overlap, there was a perceptible increase in $\delta^{18}O$ with stratigraphy. The $\delta^{18}O$ value ranged from 8.12‰ to 8.36‰ for three samples of the Campo Piedra Pomez ignimbrite, 7.63‰ for one Campo Piedra Pomez ignimbrite Plinian sample, 8.40‰–8.71‰ for the Cerro Blanco ignimbrite, and 8.35‰–8.55‰ for three samples of postcaldera domes. Based on these data, $\delta^{18}O$ is lower in the Campo Piedra Pomez ignimbrite than in the Cerro Blanco ignimbrite and postcaldera, with the highest values in the Cerro Blanco ignimbrite.

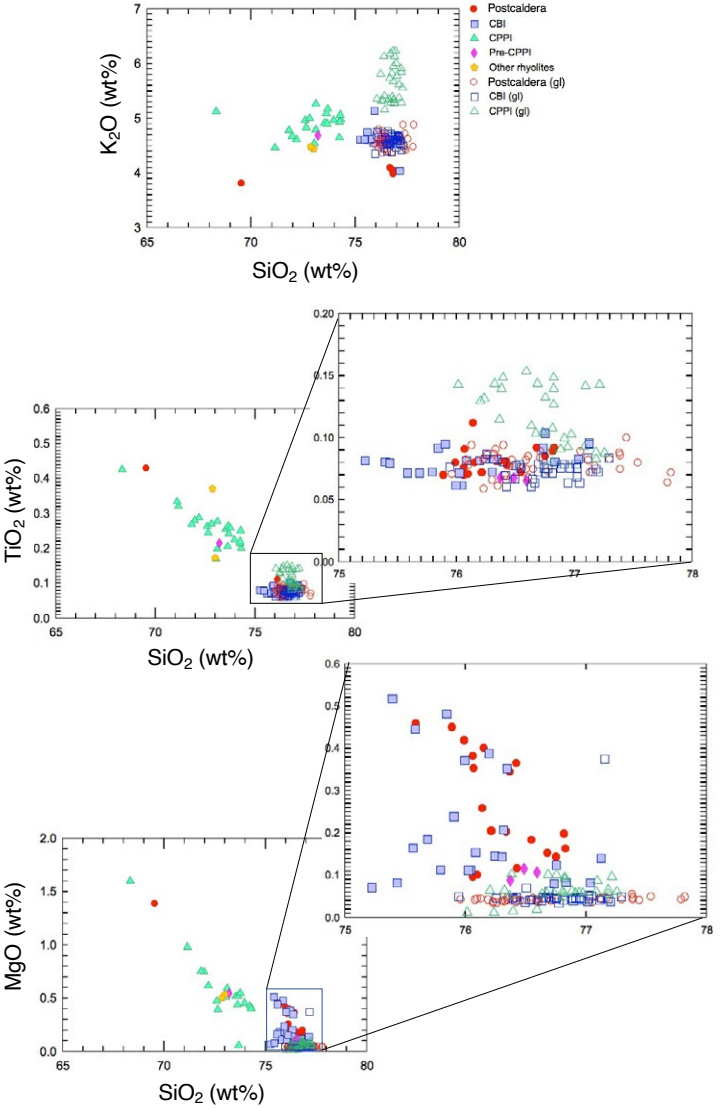

Figure 8. Selected Harker diagrams of major-element oxides for matrix glass (gl) from Cerro Blanco volcanic complex rhyolites in the context of the host bulk-rock compositions. The matrix glass variations are emphasized in the expanded boxes. Note that matrix glass data are in situ electron probe microanalysis (EPMA) spot analyses from a small subset of samples from the bulk-rock samples. CBI—Cerro Galan ignimbrite; CPPI—Campo Piedra Pomez ignimbrite.

DISCUSSION

We now return to the outstanding questions that motivated this study of the rhyolitic magmatism at the Cerro Blanco volcanic complex.

Origin of the Rhyolites as a Distinct Suite in the Southern Puna

The narrow range of isotopic compositions and their general family resemblance suggest that the rhyolitic magmas that erupted in the Cerro Blanco volcanic complex are comagmatic. These rhyolites have been previously classified as part of the southern Puna small ignimbrite suite of Siebel et al. (2001) and Schnurr et al. (2007). These regional petrogenetic studies examined regional geodynamic context and chemical diversity and demonstrated that the lower $^{87}Sr/^{86}Sr$ and higher eNd values compared with the larger-volume ignimbrites, like those from nearby Cerro Galan, reflect smaller amounts of regional basement contribution to magma genesis. They argued that the southern Puna rhyolites are the product of fractional crystallization of a large ion lithophile element–enriched andesitic parental magma, like those erupted from composite volcanoes of the arc front. The parental andesite itself is thought

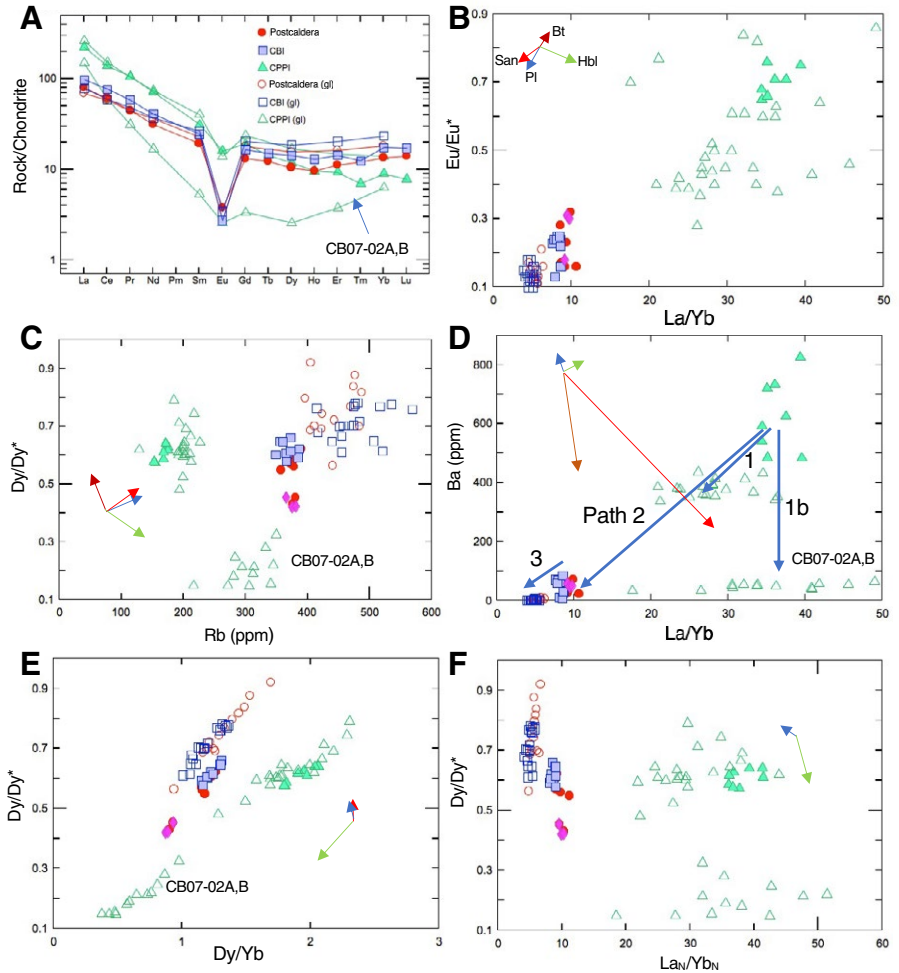

Figure 9. In situ matrix glass (gl) trace elements determined by laser ablation–inductively coupled plasma–mass spectrometry (LA-ICP-MS). (A) Chondrite-normalized rare earth elements (REE; after Sun and McDonough, 1989). Averaged data are presented here. The "anomalous" glass compositions of matrix glasses from some Campo Piedra Pomez ignimbrite Plinian fall pumice clasts are indicated by the labeled arrow. The in-situ matrix glass compositions broadly mirror the distinction seen in the bulk-rock data. (B–F) Trace-element variation diagrams for the Cerro Blanco volcanic complex. Fractional crystallization vectors for plagioclase (Pl), sanidine (San), hornblende (Hbl), and biotite (Bt) are shown, with the length of the arrows representing the impact of 10% crystallization. Titanite would mimic hornblende but would have much more leverage. Allanite would significantly fractionate the light (L) REEs and produce higher La/Yb and La_N/Yb_N. Thick arrows labeled 1–3 are the fractionation paths we modeled. D values for mineral vectors were calculated from data in Supplemental Table S8 (text footnote 1). See text for further discussion. CBI—Cerro Galan ignimbrite; CPPI—Campo Piedra Pomez ignimbrite.

to have been previously contaminated in the middle and lower crust (e.g., Davidson et al., 1991; Kay et al., 1991; Trumbull et al., 1999).

The 3–0.5 Ma Incapillo caldera and dome complex (Goss et al., 2009), the southernmost siliceous center in the Central Andes, is to date the most completely studied small siliceous center in the southern Puna. Here, siliceous magmas are distinguished by strong HREE depletion (Sm/Yb = 6–8), implicating contamination of mantle- and lower-crustal–derived magmas by partial melts of the crust at depths >40 km in the garnet stability field. Further contamination of these "adakite-like" dacitic magmas by upper-crustal melts is also indicated. Goss et al. (2010) distinguished the southern Puna ignimbrites, including the Cerro Blanco volcanic complex, from the Incapillo magmas, noting a more pronounced arc signature (e.g., La/Ta, Ba/La, and Ba/Ta) that is controlled largely by high concentrations of Ba and La in the Incapillo magmas. Another distinguishing feature is the high Sr/Yb and Sr/Y of Incapillo magmas. These distinguishing characteristics indicate that the Incapillo complex is an extreme end member of a rhyolitic caldera-forming volcano in the Puna that provides valuable context for the Cerro Blanco volcanic complex, but that is quite distinct.

We concur with the aforementioned models for regional petrogenesis and chemical diversity and do not attempt to add to the regional perspective provided earlier. We focus now on the development of rhyolitic magmas of the Cerro Blanco volcanic complex. The suggestion that "extremely evolved" magmas of the Puna region are likely crustal melts of basement composition (Drew et al., 2009) is untenable on isotopic grounds alone, as all known basement protoliths in the region (Becchio et al., 1999; Lucassen et al., 2001) are considerably more crustal than the Cerro Blanco volcanic complex and southern Puna rhyolites. Our hypothesis therefore is that the origin and internal variations in the Cerro Blanco volcanic complex are the result of AFC processes. Given the rhyolitic composition of the suite, which we will show below indicates upper-crustal pre-eruptive storage, we focused our efforts on upper-crustal processes only above ~10 km depth, following Bardelli et al. (2020), who proposed this depth, on the basis of two-pyroxene barometry, as the base of the Cerro Blanco volcanic complex rhyolitic magma reservoir. The first step is to identify end members with which to evaluate the AFC processes.

In the absence of isotopic data for the Cerro Blanco trachyandesites, and given the background of mafic volcanism throughout this region, we assumed that mafic magmas in the Antofalla–Antofagasta de la Sierra region (Thorpe et al., 1984; Drew et al., 2009; Risse et al., 2013) are reasonable parent materials to the upper-crustal systems in the southern Puna. We chose JC131, a basaltic trachyandesite (black star in Fig. 3; Fig. 7) used by Francis et al. (1989), as parental to the Cerro Galan system. It is more mafic than any of the available mafic enclaves in the Cerro Blanco system in Bardelli et al. (2020), which we would argue from regional perspectives are likely to have been precontaminated before being fed into the Cerro Blanco rhyolitic magma complex. Whereas it is likely that JC131 itself is contaminated (for constraints on the mantle-derived compositions, see discussions in Francis et al., 1989; Davidson et al., 1991; Kay et al., 1994; Trumbull et al., 1999; Drew et al., 2009; Risse et al., 2013; Maro et al., 2017; Burns et al., 2019), for our purposes of testing upper-crustal evolution, we argue that it is a reasonable local parental mafic end member.

For the crustal end member, the regional late Precambrian to early Paleozoic basement is an obvious candidate. This basement has been extensively studied to show that it is generally felsic throughout, consisting of paragneisses, orthogneisses, metasediment, granitoids, and metabasites (Becchio et al., 1999; Lucassen et al., 2001). Given the difficulty of choosing a single basement composition, we note that some authors (e.g., Drew et al., 2009) have used a "hybrid" composition of basement lithologies. We argue that nature has already completed this experiment at the large calderas like Cerro Galan, where many thousands of cubic kilometers of homogeneous siliceous magmas were produced by extensive AFC magma evolution with up to 50:50 mix of enriched mantle to crust (Kay et al., 2010a), or up to 70% using the neodymium crustal index (Folkes et al., 2013). In the immediate region of the Cerro Blanco volcanic complex and the La Hoyada, older ignimbrites include the Las Papas (9.24 ± 0.03 Ma), Aguada Alumbrera (6.82 ± 0.04–7.61 ± 0.23 Ma), and Rosada (7.09 ± 0.02 Ma) ignimbrites (Montero López et al., 2010b), and it is reasonable to assume that the host rock to the La Hoyada/Cerro Blanco volcanic complex magma system consists of these ignimbrites and their plutonic equivalents. We note the compositional similarity of the Campo Piedra Pomez ignimbrite to the local ignimbrites, including Cerro Galan and the Rosada ignimbrite (Figs. 3 and 10). The large ignimbrites show strong similarity to average basement in major- and trace-element compositions (Fig. 10D). Since isotopic data are unavailable for the Rosada and Aguada Alumbrera, and they share general characteristics with the Cerro Galan ignimbrite, for which full data sets are available, we used the Cerro Galan ignimbrite as a proxy for the crustal host rock to the Campo Piedra Pomez ignimbrite magma reservoir.

Using these two end members, we then evaluated the origin of the Cerro Blanco volcanic complex through AFC magmatic processes (DePaolo, 1981) as well as through mixing (Fig. 11). This exercise revealed that low-Si rhyolites of the Campo Piedra Pomez ignimbrite are on a bulk mixing line between the end members (model ii in Fig. 11A). The rest of the suite, the Cerro Blanco ignimbrite and postcaldera samples, have significantly higher Rb/Sr values, and the Cerro Blanco ignimbrite samples show slight but significant enrichments in $^{87}Sr/^{86}Sr$. These can be modeled with small but significant amounts of AFC at very low r (ratio of mass assimilated to mass of crystals removed) ranging from 0.025 to 0.04 (model i in Fig. 11A). The bulk distribution coefficients (D) for Rb and Sr that yielded the best-fit models were 0.001 and 3, respectively, consistent with a fractionating assemblage dominated by feldspar. We acknowledge that the D values are approximations, but they represent reasonable ballpark values for melt-crystal partitioning over a range of compositions from relatively mafic to rhyolite, but not for rhyolite to high-Si rhyolite. We will seek to refine this in future studies with more data.

An alternative shown in Figure 11A is that the large variations in Rb-Sr with very small changes in $^{87}Sr/^{86}Sr$ for the whole suite may also be modeled as due to fractional crystallization (FC) of the Campo Piedra Pomez ignimbrite magma (model iii in Fig. 11A). In this case, we can define a baseline isotopic

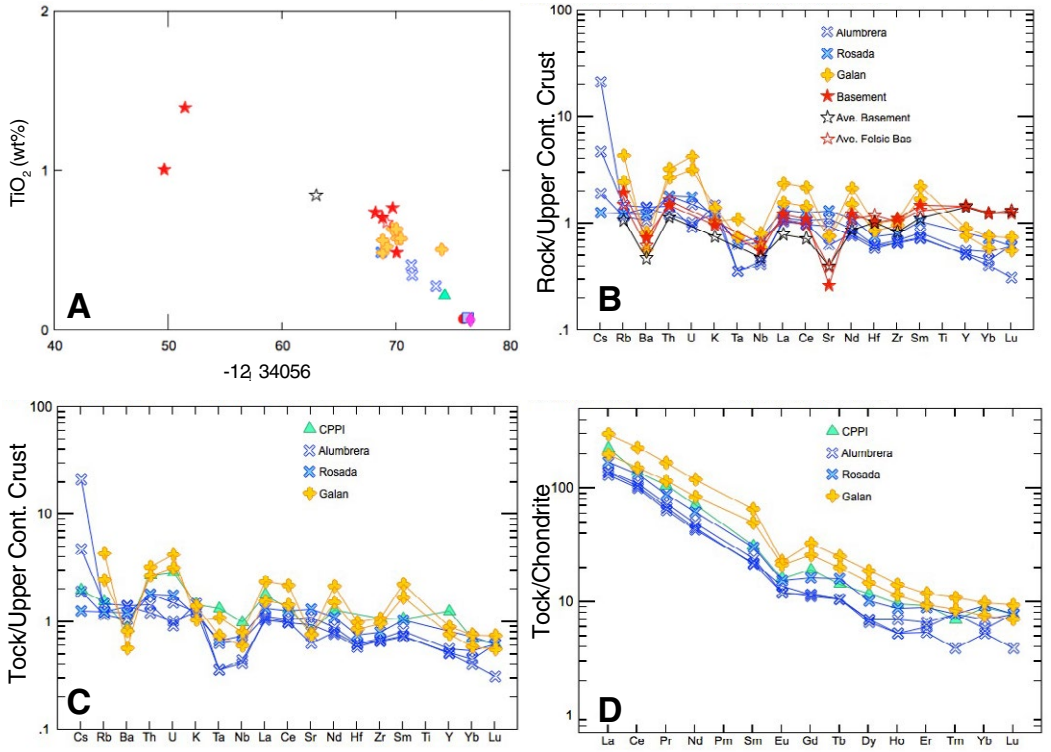

Figure 10. Constraints on a likely crustal contaminant for the Cerro Blanco volcanic complex. (A) Harker diagram for bulk rock TiO_2 vs. SiO_2 comparing average Cerro Blanco volcanic complex compositions, regional and local large ignimbrites, and basement compositions. Note the strong similarity of Cerro Galan and Rosada ignimbrite with the felsic basement compositions. (B) Upper continental crust–normalized trace-element spider diagram (Taylor and McLennan, 1985) comparing basement with regional and local large ignimbrites, showing the general family resemblance. (C) Upper continental crust–normalized trace-element spider diagram (Taylor and McLennan, 1985). (D) Chondrite-normalized rare earth element diagram (Sun and McDonough, 1989) of average Campo Piedra Pomez ignimbrite (CPPI) rhyolite with regional and local large ignimbrites, showing the general family resemblance and strong similarity of the Rosada ignimbrite to the Campo Piedra Pomez ignimbrite. See text for further discussion. Basement compositions are from Becchio et al. (1999). Other data are in Supplemental Table S2 (see text footnote 1). Symbols for Cerro Blanco volcanic complex are as in previous figures.

composition represented by the Campo Piedra Pomez ignimbrite and the postcaldera lava magmas that have indistinguishable $^{87}Sr/^{86}Sr$. The change in Rb/Sr can be produced by fractional crystallization of the Campo Piedra Pomez ignimbrite magma, and then mixing (model v in Fig. 11A) between those compositions and local, small-volume partial melts of the basement/wall rock (represented by the Cerro Galan ignimbrite; model iv in Fig. 11A) can account for the Cerro Blanco ignimbrite rhyolites with the slightly elevated $^{87}Sr/^{86}Sr$ values (Fig. 11A). So, locally, the contamination could be simply mixing with partial melts of the basement as opposed to AFC.

These models are also supported by oxygen isotope data for the Cerro Blanco volcanic complex rhyolites (Table 2B). The $\delta^{18}O$ compositions of quartz crystals from samples from the Cerro Blanco volcanic complex rhyolite suite range from 7.6‰ to 8.7‰, with an average composition of 8.3‰. These are lower than those from the Cerro Galan ignimbrite (9.3‰ average; Folkes et al., 2013) but ~1‰–2‰ higher than the melt compositions of parental basaltic andesites (as a proxy for JC131), which range from 6.7‰ to 7.2‰ (calculated from $\delta^{18}O_{olivine}$ of +6.3‰–6.8‰; Kay et al., 2010a). In $^{87}Sr/^{86}Sr$ versus $\delta^{18}O$ space, our data from the Cerro Blanco volcanic complex are well explained by AFC mixing between the two end members (Fig. 11B). The obviously lower $\delta^{18}O$ value of quartz (7.6‰) from sample CB07-2A, a sample of basal fallout from the Campo Piedra Pomez ignimbrite eruption, might indicate the local assimilation of hydrothermally altered country rock (e.g., Bindeman, 2008; Folkes et al., 2013), an idea that remains to be fully tested with a larger data set.

Our purpose with the limited isotopic data has been to establish a general set of relationships that puts the Cerro Blanco volcanic complex rhyolitic suite in the context of regional magmatism. Following others (Siebel et al., 2001; Schnurr et al., 2007; Goss and Kay, 2011), we find that the Cerro Blanco volcanic complex rhyolites can be related by AFC magmatic processes to mafic parental magmas in the southern Puna contaminated by upper-crustal basement, for which the Cerro Galan ignimbrite is a viable compositional proxy. Our data indicate that there is a baseline isotopic composition for the Cerro Blanco volcanic complex rhyolites defined by ~0.706 $^{87}Sr/^{86}Sr$ and $\delta^{18}O$ of +8.3‰. Specifically, we infer that the Campo Piedra Pomez ignimbrite rhyolite samples for which we have isotopic data are parental to younger rhyolites

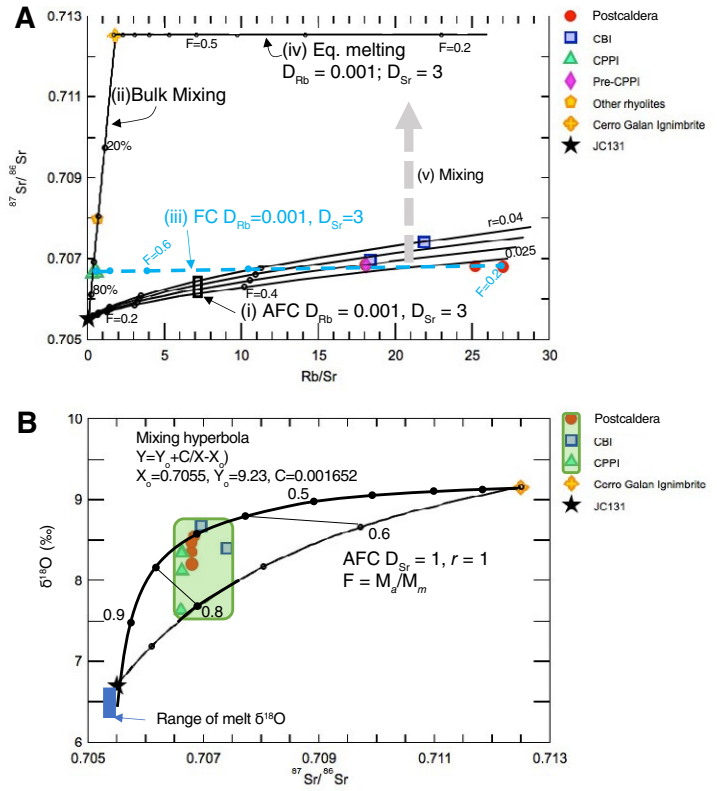

Figure 11. Models of assimilation-fractional crystallization (AFC) and mixing for Cerro Blanco volcanic complex rhyolites in isotope space. Parent magma is JC131, and basement/assimilant is the Cerro Galan ignimbrite. (A) Five models are shown: (i) $^{87}Sr/^{86}Sr$ vs. Rb/Sr with AFC curves (DePaolo, 1981) for $r = M_a/M_c$ (rate of assimilation/rate of fractional crystallization) of 0.025–0.04 and $D_{Sr} = 3$ and $D_{Rb} = 0.001$, where F = decimal fraction of AFC from 0 to 1; (ii) bulk mixing (% JC131 shown); (iii) fractional crystallization of Campo Piedra Pomez ignimbrite magma, where F = decimal fraction melt remaining; (iv) partial melting of basement (Cerro Galan ignimbrite [CGI]), where F = decimal fraction of melting; and (v) bulk mixing between magmas produced by AFC (model i) and partial melts of basement (model iv). See text for explanation of how these models are used to explain the data from the Cerro Blanco volcanic complex suite. (B) $\delta^{18}O$ vs. $^{87}Sr/^{86}Sr$ reveals that Cerro Blanco volcanic complex samples ($\delta^{18}O_{quartz}$) lie within a bulk mixing array between the end members. The mixing array is defined by two curves. The upper mixing hyperbola is a least squares mixing hyperbola implemented in IgPet (Carr and Gazel, 2017). C is the square of the residuals and a measure of the tightness of the hyperbola. The lower curve is an AFC curve where $r = 1$, $D_{Sr} = 1$ is the best fit D for Sr, M_m is the mass of original magma (JC131), and F is the relative mass of original magma (JC131/CGI). Cerro Galan data are from Folkes et al. (2013), and mafic end member is JC131 from Francis et al. (1989) for $^{87}Sr/^{86}Sr$ and Rb/Sr. Data for $\delta^{18}O_{olivine}$ are +6.7‰–6.3‰, from Kay et al. (2010a); the calculated melt composition is 6.7–7.2‰. CBI—Cerro Galan ignimbrite; CPPI—Campo Piedra Pomez ignimbrite.

with baseline isotopic compositions by fractional crystallization. Departures from this may indicate that some quartz crystals might record local mixing with small-volume partial melts of the basement.

Relationship among the Rhyolites of the Cerro Blanco Volcanic Complex—Internal Differentiation

To characterize the relationship between the Campo Piedra Pomez ignimbrite and the more evolved younger rhyolites (Cerro Blanco ignimbrite and post–Cerro Blanco ignimbrite), we used least squares modeling of major elements (Table 4). We then used the results of these models to inform models of the trace elements. Using our major-element data and published mineral compositions from the Campo Piedra Pomez ignimbrite pumice (Montero López et al., 2016; Bardelli et al., 2020), we evaluated the evolutionary pathways that cover the range of compositions for the Cerro Blanco suite. K_2O versus SiO_2 plots clearly show the differences between Campo Piedra Pomez ignimbrite and the younger rhyolites (Cerro Blanco ignimbrite and post–Cerro Blanco ignimbrite) and the differences between Campo Piedra Pomez ignimbrite whole rock and its matrix glass (Fig. 8). We divided the evolution into three paths:

(1) Campo Piedra Pomez ignimbrite magma (using sample CBV12A) to an average composition of Campo Piedra Pomez ignimbrite glass (the residual liquid),
(2) Campo Piedra Pomez ignimbrite magma (using sample CBV12A) to the Cerro Blanco ignimbrite/postcaldera magma (using sample DOMO01), and
(3) Cerro Blanco ignimbrite/post caldera magma (using sample DOMO01) to the average post–Cerro Blanco ignimbrite matrix glass (the residual liquid).

In doing so, we treated the Cerro Blanco ignimbrite and the postcaldera domes as one coherent group, a choice that is supported by their similar bulk-rock and glass chemistry. The end-member bulk-rock samples were chosen from those for which a full data set, including trace elements and isotopes, was available, and those that fell within the baseline compositions of the Sr isotopes discussed above.

The results of the least squares models are given in Table 4, and further details are available in Supplemental Table S6. These indicated the following evolutionary paths:

Path 1, from the Campo Piedra Pomez ignimbrite magma to the average Campo Piedra Pomez ignimbrite glass, can be modeled by ~7% to 15% crystal fractionation (F = 0.93–0.85) of sanidine (~41%), quartz (36%), plagioclase (12%), hornblende (5%), biotite (4%), and trace (<1%) amounts of orthopyroxene, Fe-Ti oxides, and apatite.

Path 2, from the Campo Piedra Pomez ignimbrite magma to the Cerro Blanco ignimbrite/postcaldera magma, can be modeled by ~40% crystal fractionation (F = 0.62) of sanidine (~34%), quartz (~30%), plagioclase (~16%), hornblende (~3%), biotite (~4%), Fe-Ti oxides (~2%), and trace (<1%) amounts of clinopyroxene and apatite.

TABLE 4. MAJOR-ELEMENT MODELING OF CRYSTAL FRACTIONATION FOLLOWING LEAST SQUARES MODELING APPROACH OF STORMER AND NICHOLLS (1978)

PATH 1. CPPI to average CPPI glass (F = 93%; sum of R^2 = 0.0134)

	Parent	Plag	Kfs	Qz	Hbl	Biot	Opx	Mt	Ap	Calculated	Actual	Residuals	R^2
Oxide	CBV12A	12.38%	41.34%	36.22%	5.18%	3.96%	0.67%	0.92%	0.19%		Ave glass		
SiO_2	73.93	60.6	65.52	100	47.12	37.81	56.5			76.71	76.70	–0.005	0.0000
TiO_2	0.23		0		2.23	4.97	0.07	7.51		0.14	0.12	–0.018	0.0003
Al_2O_3	13.69	24.47	18.33		8.56	14.33	0.84			13.02	13.03	0.01	0.0001
FeOtot	1.69	0.26	0.16		13.08	19.1	13.75	89.84		0.55	0.54	–0.005	0.0000
MnO	0.06		0		0.4	0.18	0.6	1.74		–0.03	0.07	0.1	0.0100
MgO	0.46		0.02		14.48	13.63	27.63	0.91		0.05	0.04	–0.007	0.0000
CaO	1.24	6.12	0.26		11.5	0.01	0.61		62.97	0.74	0.73	–0.005	0.0000
Na_2O	3.65	7.58	3.3		1.76	0.56				3.17	3.12	–0.051	0.0026
K_2O	4.97	0.96	12.4		0.88	9.4				5.65	5.63	–0.014	0.0002
P_2O_5	0.09		0			0			37.03	0.01	0.01	–0.004	0.0000
Total	100.00	99.99	99.99	100.00	100.01	99.99	100.00	100.00	100.00	100.00	100.00	0.00	0.0134

PATH 2. CPPI to postcaldera dome (F = 52%; sum of R^2 = 0.0012)

	Parent	Plag	Qz	Kfs	Hbl	Biot	Mt	Ap		Calculated	Daughter	Residuals	R^2
Oxide	CBV12A	19%	30%	45%	0.3%	3%					DOMO01		
SiO_2	73.93	58.76	100	65.95	47.12	37.81				75.896	75.898	0.00186	0.00000
TiO_2	0.23				2.23	4.97	7.51			0.098	0.070	–0.02794	0.00078
Al_2O_3	13.69	25.99		18.97	8.56	14.33				13.415	13.421	0.00635	0.00004
FeOtot	1.69	0.21		0.11	13.08	19.1	89.83			0.616	0.620	0.00443	0.00002
MnO	0.06				0.4	0.18	1.74			0.075	0.080	0.00502	0.00003
MgO	0.46				14.48	13.63	0.91			0.442	0.450	0.00815	0.00007
CaO	1.24	7.75		0.18	11.5	0.01		62.97		0.625	0.620	–0.00466	0.00002
Na_2O	3.65	6.59		3.88	1.76	0.56				4.216	4.210	–0.00578	0.00003
K_2O	4.97	0.7		10.91	0.88	9.4				4.602	4.601	–0.00145	0.00000
P_2O_5	0.09							37.03		0.017	0.030	0.01302	0.00017
Total	100	100	100	100	100	100				100.00	100.00	–0.00100	0.00116

PATH 3. CBI/PC to average matrix glass (F = 97.6%; sum of R^2 = 0.0067)

	Parent	Plag	Kfs	Qz	Hbl	Biot	Mt	Ap		Calculated	Actual	Residuals	R^2
Oxide	DOMO01	16.19%	22.01%	34.68%	16.98%	7.33%	2.68%	0.13%			Ave CBI/PC gl		
SiO_2	75.90	60.6	65.52	100	47.12	37.81				76.76	76.75	–0.003	0.000009
TiO_2	0.07				2.23	4.97	7.51			0.01	0.08	0.064	0.004096
Al_2O_3	13.42	24.47	18.33		8.56	14.33				13.29	13.28	–0.014	0.000196
FeOtot	0.62	0.26	0.16		13.08	19.1	89.84			0.48	0.48	–0.009	0.000081
MnO	0.08				0.4	0.18	1.74			0.07	0.05	–0.027	0.000729
MgO	0.45		0.02		14.48	13.63	0.91			0.11	0.09	–0.017	0.000289
CaO	0.62	6.12	0.26		11.5	0.01		62.97		0.51	0.52	0.011	0.000121
Na_2O	4.21	7.58	3.3		1.76	0.56				4.16	4.18	0.017	0.000289
K_2O	4.60	0.96	12.4		0.88	9.4				4.57	4.58	0.006	0.000036
P_2O_5	0.03							37.03		0.03	0.01	–0.029	0.000841
Total	100.00	99.99	99.99	100.00	100.01	99.99	100.00	100.00		100.00	100.00	0.00	0.006687

Note: Paths 1, 2, and 3 refer to different stages of evolution defined on Figure 10. See text and Supplemental Table S6 (text footnote 1) for further details. Mineral compositions were taken from Montero López et al. (2010a) and Bardelli et al. (2020). CBI—Cerro Blanco ignimbrite; CPPI—Campo Piedra Pomez ignimbrite; PC—postcaldera; Ave—average; Plag—Plagioclase; Kfs—Sanidine; Qz—Quartz; Hbl—Amphibole; Biot—Biotite; Opx—Orthopyroxene; Mt—Magnetite; Ap—Apatite; gl—glass. Major oxides are given in wt%.

Path 3, from the Cerro Blanco ignimbrite/postcaldera magma to the average postcaldera glass compositions, representing internal differentiation of the Cerro Blanco ignimbrite and postcaldera dome magma, can be modeled with ~2%–3% crystal fractionation (F = 0.97–0.98) of quartz (35%), sanidine (~22%), hornblende (17%), plagioclase (16%), biotite (7%), Fe-Ti oxides (3%), and trace amounts of apatite. If orthopyroxene is included in the model, then this replaces some amphibole and increases the amount of plagioclase.

These models illustrate that the suite of siliceous magmas at Cerro Blanco volcanic complex can be related to each other through crystal fractionation of observed phenocryst phases. The model proportions are reasonable and yield bulk distribution coefficients (D_{Sr} ~3; D_{Rb} = 0.01) consistent with the FC and AFC calculations we presented above obtained from the isotopic data. Again, we acknowledge that these are ballpark values for averages of melt-crystal partitioning over a range of compositions from relatively mafic to rhyolites, but not for rhyolites and high-Si rhyolites. An important inconsistency between model and observation is that the predicted amount of crystallization and the proportions are not always consistent with modal estimations; for instance, the Campo Piedra Pomez ignimbrite pumice has crystal contents that range from 5% to 20% (rarely), and the Cerro Blanco ignimbrite pumice typically has 2%–3%, with 5% being rare. This discordance is not uncommon in high-silica magmas, as modal contents often do not reflect the full record of the fractionating mass (e.g., Michael, 1983; Miller and Mittlefehldt, 1984; de Silva and Wolff, 1995). Noting that among the most evolved compositions, the postcaldera domes contain up to 50% crystals, we return to this discordance below.

Building on the major elements, we looked at the trace elements to validate our fractional crystallization models. We used a series of multi-element "spider" diagrams to illustrate the modeled relationships between daughter melts represented by the matrix glass and parent CBV12A (path 1 above; see Fig. 9), informed by the assemblage modeled in the least squares modeling of the major elements (Fig. 12). A good fit between model daughter and actual daughter (DOMO01) was obtained for models with F = 0.55–0.45, consistent with the major-elements models (Supplemental Table S9). The main departure was the inability to reproduce the higher U and Cs contents of the daughter, a failure that we attribute to choice of mineral *Kd* values and their impact on the bulk D values, the lack of assimilation or the incorporation of local partial melts in these models, and unmodeled accessory phases. Still, despite this small inconsistency, it is clear that the samples with baseline isotopic compositions of the Cerro Blanco volcanic complex can be related to each other by fractional crystallization of a host Campo Piedra Pomez ignimbrite magma composition, in this case represented by CBV12A. Differentiation in

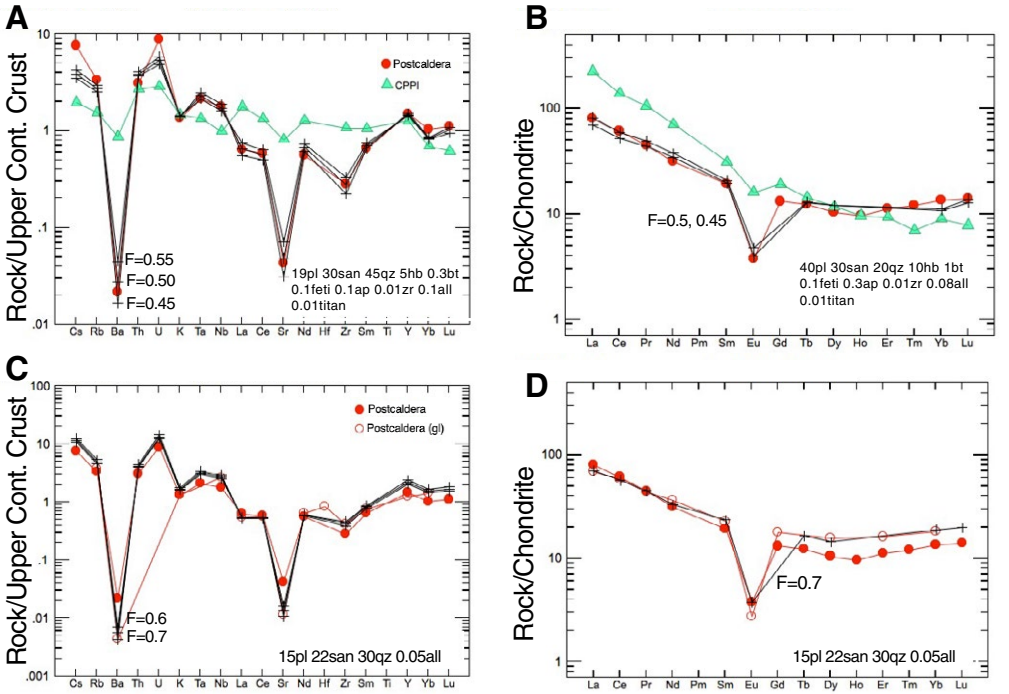

Figure 12. Multi-element spider diagrams with Rayleigh fractionation models of Cerro Blanco volcanic complex rhyolites. Rock/upper continental crust normalization is after Taylor and McLennan (1985); rock/chondrite normalization of rare earth elements (REEs) is after Sun and McDonough (1989). The fractionating assemblage is given in each panel, and F is the fraction of melt remaining. (A–B) Path 2 in Figure 9—Bulk-rock Campo Piedra Pomez ignimbrite (CPPI; sample CBV12A) to bulk-rock postcaldera dome (DOMO01). Note that the assemblage in panel A is that derived from the least squares model for the same parent and daughter (Table 4). (C–D) Path 3 in Figure 9—Bulk-rock DOMO01 to average postcaldera matrix glass (gl) in situ data from laser ablation–inductively coupled plasma–mass spectrometry (LA-ICP-MS). See text for interpretation of these diagrams. The models were derived using Rayleigh fractionation equations built into IgPet™ petrological modeling software (Carr and Gazel, 2017) and the mineral-melt distribution coefficients from Supplemental Table S8 (see text footnote 1). The calculated bulk distribution coefficients for each model and F values are also compiled in the Supplemental Table S9 (see text footnote 1) and discussed in the text. Abbreviations: pl—plagioclase; san—sanidine; qz—quartz; hb—hornblende; bt—biotite; feti—Fe-Ti oxides; ap—apatite; zr—zircon; all—allanite; titan—titanite.

the most-evolved compositions from DOMO01 to average postcaldera glass compositions (path 3 above; see Fig. 9) was also assessed. A good fit between model daughter and actual daughter (DOMO01) was obtained for models with F = 0.7–0.6, consistent with the major-element models. This path is distinct from the major-element models in not only the lack of emphasis on amphibole and mafic phases, but also the amount of fractionation: 2%–3% for the major elements, and 30%–40% for the trace elements. This again is not unusual for minimum melt compositions where fractionation can produce significant variations in trace elements for buffered major-element composition; we deal with this disconnect below.

An interesting nuance in the in situ matrix glass data set is the bimodal trace-element compositions exhibited by matrix glass from Campo Piedra Pomez ignimbrite pumice (Figs. 9 and 13). The glasses from two pumice samples of the basal Plinian fallout (samples CB07-2A and CB07-2B) share a general family resemblance to the other Plinian fall sample and Campo Piedra Pomez ignimbrite pumice in bulk chemical properties. Chondrite-normalized REE patterns of pumice matrix glass from two different samples of the pumice fall (samples CB07-02A and CB07-02B) show a pronounced depletion of the MREEs, resulting in a deep concavity to the pattern (note that this is seen in all 30 spot analyses and does not reflect a single spot analysis of a wayward crystal). This anomaly can be quantified by the Dy/Dy* measure of Davidson et al. (2012), who attributed a concave pattern to the fractionation of amphibole or clinopyroxene, which have a strong affinity for the MREEs. We note that titanite is also extremely effective in producing this pattern in the REEs, but since amphibole is present as a phenocryst in the Cerro Blanco volcanic complex, we focus on this mineral.

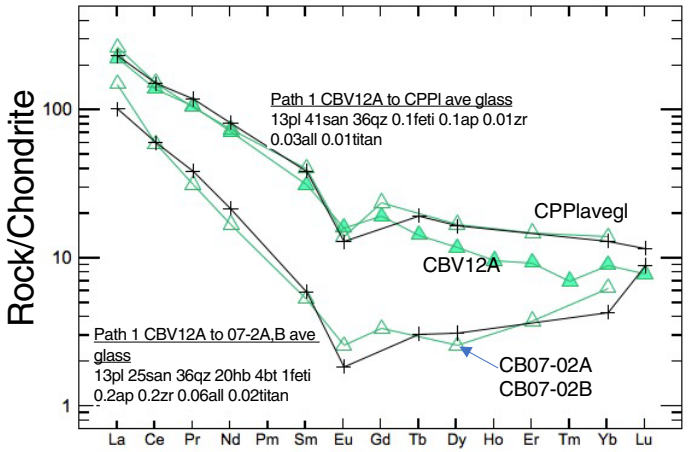

Figure 13. Rayleigh fractional crystallization models for internal fractionation with the Campo Piedra Pomez ignimbrite rhyolites. These models evaluate paths 1 and 1b on Figure 9 and attempt to account for internal variation seen for in situ matrix glass (gl) analyses within the Campo Piedra Pomez ignimbrite (CPPI). The fractionation assemblage for each model is shown. See text for interpretation of these diagrams. The models were derived using Rayleigh fractionation equations built into IgPet™ petrological modeling software (Carr and Gazel, 2017) and the mineral-melt distribution coefficients from literature sources compiled in Supplemental Table S8 (see text footnote 1). The calculated bulk distribution coefficients for each model and F values are compiled in Supplemental Table S9 (see text footnote 1) and discussed in the text. Mineral abbreviations as in Figure 12.

On plots with Dy/Dy* (Fig. 9), it is clear that the matrix glass in the CB07-02A and CB07-02B samples is characterized by extremely low Dy/Dy* compared to all the other samples for which we have data; the rest of the Cerro Blanco suite has Dy/Dy* >0.4, with most of the population being above 0.5. Rayleigh fractionation models indicate that this group of CB07-02A and CB07-02B matrix glasses could have been derived from the parental CBV12A through ~55% crystal fractionation (F = 0.45) of an assemblage in which amphibole was ~20% of the fractionating assemblage (path 1b in Fig. 13; Supplemental Table S9). This contrasts with the more typical sanidine-plagioclase-quartz–dominated assemblage that would yield the typical matrix glass in the Campo Piedra Pomez ignimbrite (path 1 in Fig. 13). Note that the bulk D values for the REEs in the two models are quite different, reflecting that an assemblage rich in REE-bearing phases, such as titanite, in addition to amphibole is required. However, we emphasize the role that can be played by fractionation of amphibole in nonmodal amounts. Amphibole-rich cumulate inclusions are a ubiquitous feature in pumices from the Central Andes and have been shown to have strongly upward-convex REE patterns consistent with MREE sequestration in amphibole (de Silva, 1989). These patterns are complementary to the concave patterns seen in CB07-02A and CB07-02B. We therefore emphasize the role of cryptic amphibole fractionation in producing the REE characteristics of this particular horizon in the Campo Piedra Pomez ignimbrite stratigraphy.

These characteristics connote that the CB07-02 matrix glass might represent a pod of distinct melt where amphibole was saturated relative to the feldspars, particularly sanidine. Grocke et al. (2017a) demonstrated experimentally that lower pressure and lower water contents controlled the relative stability of sanidine and amphibole at Cerro Galan, with sanidine appearing at lower pressure and lower water contents. Given that sanidine appears to be ubiquitous in the Cerro Blanco suite, we propose that CB07-02 samples represent a pod of melt that fractionated from a relatively wet magma that promoted amphibole and REE-bearing phases.

Overall, these models of classical Rayleigh fractionation connote an origin through crystal fractionation from a parental rhyolite of Campo Piedra Pomez ignimbrite composition. In this case, we have used CBV12-A as the parent and DOMO01 as the daughter. Associated glasses have been used as the residual liquids that represent the final products of fractionation. Whereas we recognize that the models are not exclusive, they still provide useful first-order constraints that can be tested with more data in the future. Our working hypothesis is that progressive evolution from the Campo Piedra Pomez ignimbrite magma to the postcaldera glass was dominated by fractional crystallization and could

have progressed in multiple stages during the ~54 k.y. eruptive history of the Cerro Blanco volcanic complex.

Pressure-Temperature Conditions of Pre-Eruptive Storage and Architecture of the Magmatic Complex

Various estimates of pressure–temperature–water content (*P-T*-H_2O) for the Cerro Blanco volcanic complex have been determined by previous work. Pre-eruptive H_2O contents measured in quartz-hosted melt inclusions range from 1.1 to 8.6 wt% (Roberge et al., 2018). Magmatic temperatures of around 760–820 °C and 600–750 °C from Fe-Ti oxide equilibria have been estimated for the Campo Piedra Pomez ignimbrite and Cerro Blanco ignimbrite, respectively (Báez, 2015; Fernández-Turiel et al., 2019). Bardelli et al. (2020) used two-pyroxene geobarometry to constrain the base of the Campo Piedra Pomez ignimbrite magma complex to be near 10 km depth (2.6–2.7 kbar), and they interpreted this to be a zone of extensive interaction between recharging mafic magma and the main rhyolitic magma. We provide a new perspective here.

We have established above that the Campo Piedra Pomez ignimbrite is dominated by a quartz-plagioclase-sanidine phase assemblage. In combination with high-silica rhyolite compositions of the melts (>76% to 78% SiO_2), this phase assemblage requires a shallow (<300 MPa) environment of magma storage and evolution (e.g., Blundy and Cashman, 2001; Gualda and Ghiorso, 2013). The matrix glass (residual melt) compositions projected onto the synthetic system quartz-albite-orthoclase-H_2O (Qz-Ab-Or-H_2O) can reveal the last conditions of equilibrium between crystals and melt (e.g., Tuttle and Bowen, 1958; Johannes and Holtz, 1996; Blundy and Cashman, 2001; Gualda and Ghiorso, 2013). In this silica-rich part of Bowen's petrogeny's residua (Bowen, 1937), the silica content of melts increases with decreasing pressure as a result of the displacement of the quartz-feldspar cotectic toward the quartz apex with decreasing pressure (Gualda and Ghiorso, 2013).

Following these experimental studies, we assessed the pressure-temperature-composition (*P-T-X*) record of the Cerro Blanco volcanic complex rhyolite melts (Fig. 14) using the scheme of Blundy and Cashman (2001). These

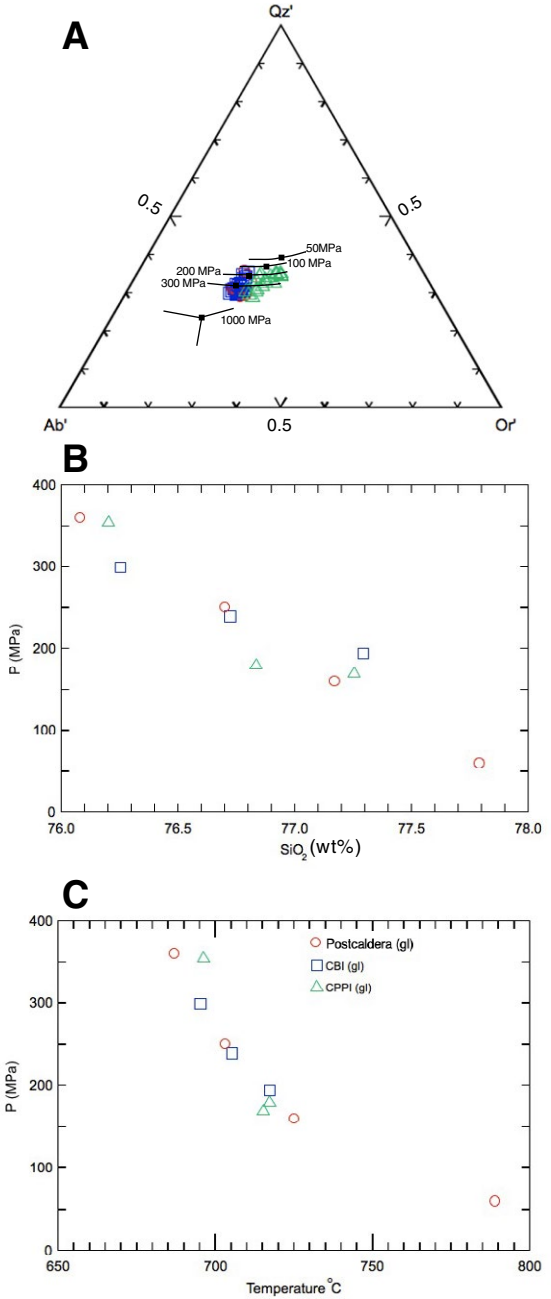

Figure 14. Pressures and temperatures of equilibration of matrix glass compositions from the Cerro Blanco volcanic complex rhyolite suite. (A) Projection of average matrix glass compositions onto the synthetic haplogranitic system (quartz [Qz]–albite [Ab]–orthoclase [Or]–H_2O; Johannes and Holtz, 1996). Cotectics are from Blundy and Cashman (2001, and references therein). Matrix glass normative compositions were corrected according the procedure detailed in Blundy and Cashman (2001) and are compiled in Supplemental Table S7 (see text footnote 1). (B–C) Pressure-temperature-SiO_2 relationships of maximum, minimum, and average matrix glass compositions calculated with rhyolite-MELTS. The temperatures shown here have been adjusted by –40 °C from the model temperatures retrieved from rhyolite-MELTS as recommended in Gualda et al. (2012). Symbols are the same as in Figure 9. CBI—Cerro Galan ignimbrite; CPPI—Campo Piedra Pomez ignimbrite; gl—glass.

are all slightly different flavors of high-Si rhyolite with SiO_2 ranging from >76% to almost 78%. Projection of the glass compositions onto the Qz-Ab-Or part of petrogeny's residua reveals that these melt compositions equilibrated at pressures of ~300 MPa to <100 MPa or depths of ~10 km to <3.5 km for typical crustal densities in this region (Fig. 14A). Campo Piedra Pomez ignimbrite glasses are displaced toward the Or apex compared to the Cerro Blanco ignimbrite/postcaldera group.

To verify these graphical estimates, we ran simple models using rhyolite-MELTS to check the *P-T* conditions where feldspars and quartz equilibrate for the various melt compositions (Figs. 14B and 14C). The results of the MELTS models (Fig. 14B) revealed pressures ranging from 360 to 60 MPa, in general agreement with the graphical estimates. In running these models, we assumed H_2O saturation of the melts, which seems reasonable given the presence of both amphibole and biotite in these magmas. Moreover, reconnaissance data indicated that dissolved H_2O contents in quartz-hosted melt inclusions vary from 1.1 to 8.6 wt% (Roberge et al., 2018), and a range 4–6 wt% was also derived from the plagioclase-glass hygrometer of Lange et al. (2009).

Temperatures estimates in MELTS models ranged from 687 °C to 789 °C and were inversely correlated with pressure. This is because liquidus temperatures increase rapidly with decreasing pressure due to the pressure dependence of water solubility (e.g., Rutherford and Hill, 1993; Blundy and Cashman, 2001; Gardner at al., 2014). We discuss the potential implications of this below.

One of the nuances of the R-MELTS model results is that the lowest pressures and depths are one feldspar–quartz solutions as opposed to the two feldspar–quartz solutions of the other pressures. This appears to be function of the elevated K_2O/Na_2O in the most-evolved glass composition from the postcaldera domes. We believe these are real and not analytical effects where Na is lost due to volatilization because our analytical methods were designed to limit sodium loss, and only some of the most Si-rich matrix glasses from the postcaldera domes show this effect. We are confident in the analyses and the veracity of the pressures because they correlate well with the graphical projections, but they nevertheless require some explanation. We noted above that unlike the pumices of the Cerro Blanco volcanic complex rhyolites, which are hyalohaline, the postcaldera lava samples are characterized by the presence of abundant microlites in the groundmass. The microlites are primarily plagioclase, and we propose that the elevated K_2O in these matrix glasses reflects this late-stage crystallization. We therefore interpret the higher SiO_2 contents and the lower pressures to reflect ascent from shallow levels <100 MPa under large undercooling conditions that promoted nucleation (e.g., Blundy and Cashman, 2001); rapid ascent from such shallow levels would result in a hyalohaline matrix as seen in the explosive Cerro Blanco ignimbrite and fall unit. One consequence of groundmass crystallization is release of latent heat of crystallization, which can result in the temperature of ascending magma increasing by up to 100 °C (e.g., Blundy et al., 2006; Pallister et al., 2008), and this may have facilitated the eruption of the crystal-rich magma through bubble growth and melt viscosity changes (Okumura et al., 2019). Testing these ideas will have to wait until more detailed petrological studies are undertaken.

Temporal Evolution of the Cerro Blanco Volcanic Complex Magma System

We now integrate our results and interpretations into a working model for the evolution of the Cerro Blanco volcanic complex with time. The available matrix glass data constrain the magma complex to be between ~60 and 300 MPa, or ~2.2 and 10 km depth. The base of the siliceous complex where interaction among rhyolitic and mafic magmas of the Campo Piedra Pomez ignimbrite occurred has been proposed to be at a depth of 10 km (260–270 MPa; Bardelli et al., 2020). Each of the eruptions of rhyolitic magma contained melts that equilibrated throughout the vertical extent of the magma column, although the most recent eruption records the lowest pressures.

Based on these constraints, we envisage a vertically extended magma complex built within a basement of regional ignimbrite (Fig. 15). Millions of years of andesitic magmatism of the La Hoyada volcanic complex have also emplaced various small plutons that are likely tonalitic in composition. For simplicity, these are ignored, and the entire basement is assumed to be regional ignimbrite like the Las Papas, Aguada Alumbrera, Rosada, or the Cerro Galan ignimbrite. In our starting stage, an andesitic magma derived from a parent like basaltic andesite JC131 evolved through AFC magmatic processes at 10–11 km or so (Fig. 15A). This andesitic reservoir was the engine for the Cerro Blanco magmatic complex, providing both heat and mass, and it was maintained by a continued magma flux from below. Over time, the andesite differentiated through fractional crystallization along with assimilation to produce the main mass of Campo Piedra Pomez ignimbrite rhyolite. At the base of the growing rhyolite, at ~10 km, andesitic magma recharged the system, and induced local assimilation of the ignimbrite country rock, providing some enrichment in $^{87}Sr/^{86}Sr$ and $\delta^{18}O$ and depletion of eNd, and establishing the Pb isotopic signature of the magmas. This created the "baseline" compositions of the Cerro Blanco volcanic complex siliceous magmas prior to the Campo Piedra Pomez ignimbrite eruption. As the rhyolite mass grew and propagated upward, early leaks from this growing rhyolite mass may be recorded in the pre–Campo Piedra Pomez ignimbrite eruptions, for which we have very little data, but those we do have indicate the full spectrum of rhyolites is represented in this stage, and both Campo Piedra Pomez ignimbrite and Cerro Blanco ignimbrite/postcaldera types were erupted. These were probably homogenized into the large growing mass of Campo Piedra Pomez ignimbrite over time. Internal differentiation of the Campo Piedra Pomez ignimbrite magma progressed through fractional crystallization predominantly, along with local mixing and assimilation of basement, to produce the evolved matrix glass compositions. We can further constrain the nature of this magma complex through some geological considerations and simple first-order calculations.

Two spatially separate caldera collapses have been proposed for the two major eruptions—those of the Campo Piedra Pomez ignimbrite (<54 ka) and the Cerro Blanco ignimbrite (4.2 ka) (Báez et al., 2020a, 2020b). This constraint has to be integrated with our demonstration of the comagmatic relationship

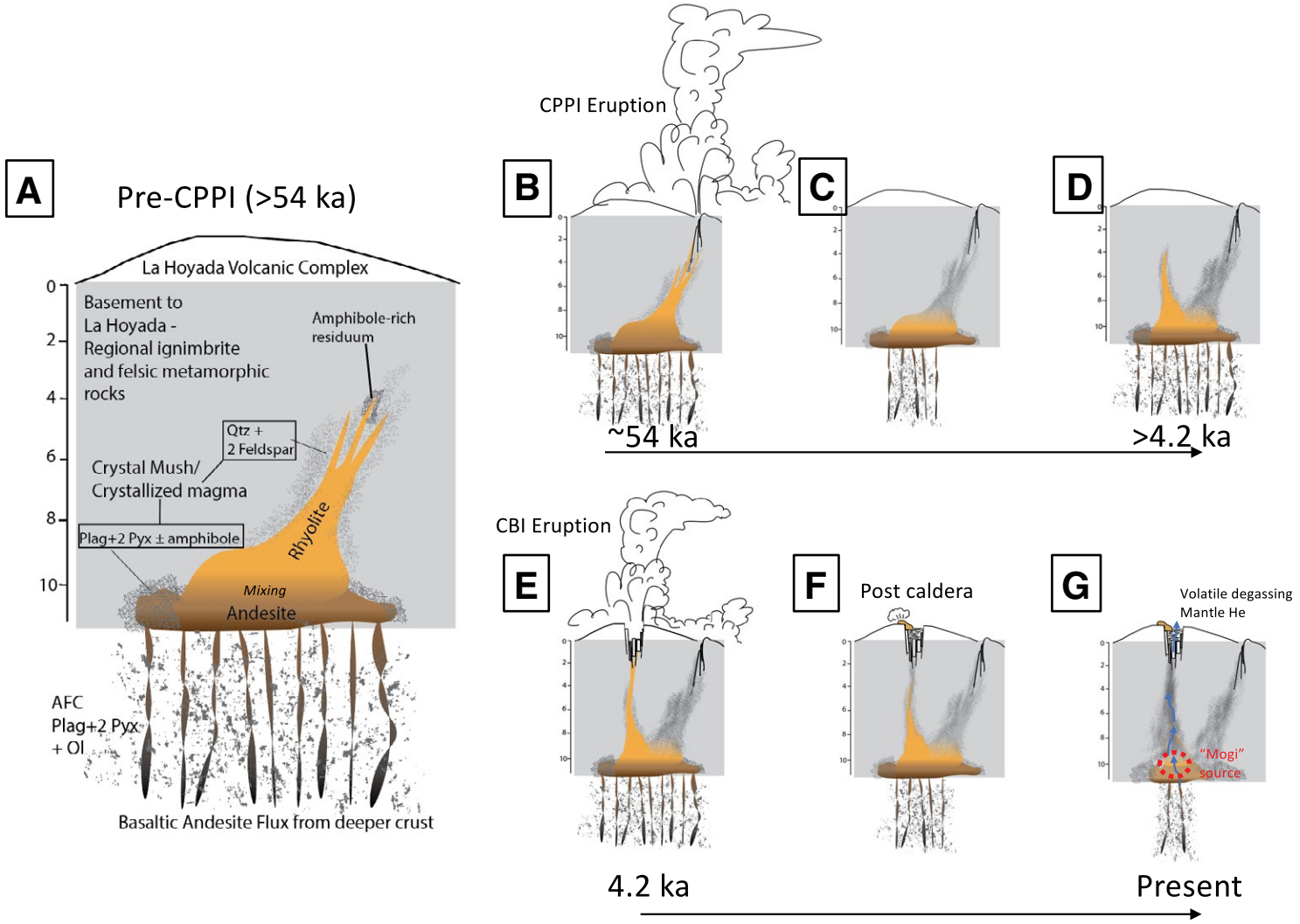

Figure 15. Working model for the late Pleistocene to recent magma dynamics of the Cerro Blanco volcanic complex. View is toward the west. Vertical scale is ~2× horizontal scale. (A) Older than 54 ka, pre–Campo Piedra Pomez ignimbrite (CPPI) magmatic and volcanic architecture. Basement to La Hoyada is shown as a monotonous regional ignimbrite lithology. The La Hoyada plutonic system is not shown for simplicity. This panel also acts as a legend, to which the subsequent panels can be referenced. Qtz—quartz; Plag—plagioclase; Pyx—pyroxene; AFC—assimilation and fractional crystallization; Ol—olivine. (B) Circa 54 ka. The Campo Piedra Pomez ignimbrite Plinian eruption and formation of the Pie de Buenaventura–El Nino caldera. (C) Post–Campo Piedra Pomez ignimbrite cooling and solidification of the Campo Piedra Pomez ignimbrite plutonic apophysis. Waning deep mafic magma flux. (D) More than 4200 yr ago. Development of the pre–Cerro Blanco ignimbrite (CBI) magma apophysis. Waxing deep magma flux. (E) Circa 4200 yr ago. The Cerro Blanco ignimbrite Plinian eruption and formation of the Cerro Blanco caldera. (F) <4200 yr ago to recent. Postcaldera dome effusions and local pyroclastic flows (block-and-ash flows) onto intracaldera fill. Waning deep magmatic flux. (G) Present day. Much of the rhyolitic magma is solidified, and only a small portion of the basal andesitic/rhyolitic reservoir remains melt dominated, heated by continued but waning deep mafic flux. Mantle-derived volatiles percolate upward and exhale through the active hydrothermal system. Approximate location of the deformation (Mogi) source is shown. See text for further details.

of the rhyolites and the parental role for the Campo Piedra Pomez ignimbrite rhyolite. We therefore propose two separate magma columns or apophyses, one under each of the calderas, but connected at depth by a large zone of Campo Piedra Pomez ignimbrite rhyolite parental magma above the basal recharge zone. The vertical extents of the magma columns are ~8 km (2–10 km), based on the pressure estimates. Assuming that these are cylinders with cross-sectional area of the Cerro Blanco caldera (average radius = 2.25, area = 15.5 km^2), the total volume of each of these columns would be ~125 km^3. The known erupted magma volumes of Campo Piedra Pomez ignimbrite and Cerro Blanco ignimbrite eruptions are ~10 km^3 (current estimates in Báez et al., 2020a, 2020b), but they could be as high as 30 km^3 due to poor knowledge of the distal ash component (see Fernández-Turiel et al., 2019; Báez et al., 2020b). For each eruption, if all this magma was siphoned from an all-melt magma column, then the volume loss extracted equates to a column depth of ~600 m to ~2 km. However, since the matrix glasses record the full 8 km range of pressures, this requires that melts from all that range were erupted. This implies a magma column that was composed of 10%–25% by volume interconnected, largely crystal-poor rhyolitic melt. This could be disseminated as pods of disconnected magma or a connected zone of melt, both within a mushy framework. We argue that without knowledge of the heat flux from depth and thermal history of the magma complex, the most thermally viable configuration for such a small fraction of melt to remain eruptible is in the form of a continuous melt-rich conduit rather than individual small pods of melt at different depths. Connectivity to the thermal source at the base of the system would be paramount in keeping this system viable over the depth range represented. Given the modeled amounts of fractional crystallization required to reproduce the major- and trace-element characteristics of the rhyolites, the rest of the magma column must have been composed of cumulates, and the whole column can be thought of as a mush column with a central core of interconnected melt. These considerations inform our current conceptualization of the Cerro Blanco magma system (Fig. 15).

Prior to the Campo Piedra Pomez ignimbrite eruption (ca. 54 ka), a northerly apophysis developed beneath the arc of the Pie de San Buenaventura and El Nino collapse scarps and was tapped by the Campo Piedra Pomez ignimbrite eruption (Fig. 15B). Most of this solidified into a pluton, but the lower parts that were fed by recharge remained melt-rich (Fig. 15C). The melt flux from depth may have waned during this time.

Some time before 4200 yr ago, prior to the Cerro Blanco ignimbrite eruption, a magma column began to grow a few kilometers to the south under the location of the future Cerro Blanco caldera (Fig. 15D). This may have been fueled by an increase in the melt flux from deep beneath the andesitic reservoir. Fed by remnant Campo Piedra Pomez ignimbrite magma that then fractionated along path 2 described above, the Cerro Blanco ignimbrite magma was generated (Fig. 15D).

Throughout these stages, evolved melt from the mush fractionated upward through local buoyancy effects and was mixed with melt derived from marginal zones of crystallization and local melting of country rock that produced small departures from baseline isotopic compositions (model v on Fig. 11). The magma column extended upward and initiated the Cerro Blanco ignimbrite eruption. Eruption of this southerly magma column occurred at 4.2 ka, accompanied by collapse of the Cerro Blanco caldera, which filled with intracaldera ignimbrite (Fig. 15E).

After the Cerro Blanco ignimbrite eruption, a dominantly mushy magma column was left, and this was augmented by recharging andesite at the base of the column to erupt effusively as lava domes and local pyroclastic flows (Fig. 15F). Ascent from the shallowest levels resulted in decompression crystallization and the formation of microlites and associated heating and vesiculation, which may have helped erupt the crystal-rich magma (e.g., Okumura et al., 2019). Domes and explosion craters formed on the rim and outside the caldera, while block-and-ash flows collected within the caldera collapse zone.

Currently, the Cerro Blanco magma complex is assumed to be largely crystallized, but it remains actively recharging today at depth, as indicated by the relatively high fraction of mantle He (calculated to be ~39% on the basis of the measured R/Ra values[2]; Chiodi et al., 2019). This thermal source maintains the small but active hydrothermal system. The decades of deflation detected in the caldera may reflect the progressive solidification of the magma complex into a vertically composite Cerro Blanco tonalite-granodiorite-granite pluton (Fig. 15G).

CONCLUSIONS

The Cerro Blanco volcanic complex is a Crater Lake–type, late Pleistocene to Holocene, rhyolitic caldera complex in the southern Puna Plateau of the Central Andes of Argentina. The siliceous magmatism here is typical of caldera-forming volcanic complexes in steady-state (normal mantle flux) arcs. It has been the site of two VEI 6 caldera-forming eruptions that emplaced the ca. 54 ka Campo Piedra Pomez ignimbrite and the ca. 4.2 ka Cerro Blanco ignimbrite and formed separate calderas. As such, it is the most productive recent explosive volcano in the Central Andes. The most recent eruptions are dominantly effusive postcaldera domes and associated small explosive phases.

The Cerro Blanco volcanic complex is the surface expression of a rhyolite-dominated (73–76% SiO_2) magma complex that initiated >54 k.y. ago and has since waxed (caldera-forming) and waned (intercaldera). It remains potentially active to the present day, fed by andesite recharge at ~10 km depth. New isotopic data indicate that the Cerro Blanco volcanic complex rhyolite suite is part of a regional southern Puna small ignimbrite group that is distinct from the large ignimbrites that were erupted during the Neogene flare-up in the Central Andes. The rhyolite magmas are the product of limited assimilation of local basement by andesites followed by extensive fractional crystallization

[2]The $^3He/^4He$ ratio (R) is usually used as a proxy for ^3He content. R is generally expressed as a multiple of the present-day atmospheric $^3He/^4He$ ratio, Ra, which is 1.38 x 10^{-6}.

(AFC). The andesites themselves are the result of AFC processes in parental regional basaltic andesites.

The initial rhyolites were low-Si rhyolites of the Campo Piedra Pomez ignimbrite, from which the younger rhyolites could have been derived by extensive nonmodal fractionation of a quartz–two feldspar (granitic minimum) assemblage with minor assimilation. Some distinct melt compositions in the Campo Piedra Pomez ignimbrite require extensive fractionation of amphibole. Distinct matrix glass compositions of the Campo Piedra Pomez ignimbrite and Cerro Blanco ignimbrite can be used as geochemical fingerprints for tephrochronology. Available data indicate that rhyolites from other neighborhood centers such as Cueros de Purulla share chemical characteristics with the Campo Piedra Pomez ignimbrite rhyolites, but they also appear to be isotopically distinct.

Pre-eruptive storage and final equilibration of matrix glass compositions are estimated between ~300 and 60 MPa (~10–2.2 km depth), with the lowest pressures in the most recent eruptions. Overall, a polybaric evolution of siliceous magmas beneath the Cerro Blanco volcanic complex is indicated, with gradual shallowing of the magmatic complex. Final equilibration of some of the postcaldera domes during ascent and decompression occurred at depths <2 km.

Geochemical models imply significant volumes of remnant felsic and intermediate-composition cumulates, and we propose that a composite, incrementally accumulated (over ~54 k.y.), granitic to tonalitic pluton has developed between ~2 km and at least 10 km depth beneath the Cerro Blanco volcanic complex. The volume decrease associated with progressive solidification of the magma complex may account for the decades of deflation (e.g., Henderson and Pritchard, 2013) that have been measured at Cerro Blanco. The two cycles of explosive caldera-forming activity may reflect cyclicity in the deep thermal flux from the lower crust and/or mantle. The presently active geothermal anomaly and hydrothermal springs indicate that the Cerro Blanco volcanic complex remains potentially active today, although the magmatic system may be in a waning stage.

ACKNOWLEDGMENTS

We are grateful to Universidad Nacional de Salta, the former Instituto de Geología del Noroeste Argentino (GEONORTE), and Instituto de Bio y Geociencias del Noroeste Argentino (IBIGEO, CONICET) for logistic support during the field work. We also acknowledge Rufino Lozano for the X-ray fluorescence (XRF) analysis at the Laboratorio Universitario de Geoquimica Isotopica (LUGIS) at Universidad Nacional Autónoma de México and Frank Tepley and Dale Burns for their assistance with microprobe analysis at Oregon State University. We thank Adam Kent for his assistance with the laser ablation–inductively coupled plasma–mass spectrometry (ICP-MS) at Oregon State University, Ilya Bindeman (University of Oregon) for the O isotope analyses, and Frank Ramos (New Mexico State University) for the radiogenic isotope analyses. Gerardo Arrieta-Garcia is also thanked for his comments on parts of this manuscript. Field logistical support by Cristian Metzke and Alma Gaucho is fully appreciated. Financial support for work in the Cerro Blanco region was provided by grant PIP 0247 from Consejo Nacional de Investigaciones Científicas y Técnicas (CONICET), Argentina, Consejo de Investigación Universidad Nacional de Salta (CIUNSa) Program, U.S. National Science Foundation grant EAR-0710545, and National Aeronautics and Space Administration grants MFRP NNX10AP79G and 16-SSW16_2–0141. Insightful and thorough reviews by two anonymous reviewers, Calvin Miller, and the *Geosphere* guest associate editor improved this paper considerably.

REFERENCES CITED

Acocella, V., Gioncada, A., Omarini, R., Riller, U., Mazzuoli, R., and Vezzoli, L., 2011, Tectonomagmatic characteristics of the back-arc portion of the Calama–Olacapato–El Toro fault zone, Central Andes: Tectonics, v. 30, TC3005, https://doi.org/10.1029/2010TC002854.

Allmendinger, R.W., Jordan, T.E., Kay, S.M., and Isacks, B.L., 1997, The evolution of the Altiplano-Puna plateau of the Central Andes: Annual Review of Earth and Planetary Sciences, v. 25, no. 1, p. 139–174, https://doi.org/10.1146/annurev.earth.25.1.139.

Arnosio, M., Becchio, R., Viramonte, J.G., Groppelli, G., Norini, G., and Corazzato, C., 2005, Geología del Complejo Volcánico Cerro Blanco (26°45′LS, 67°45′LO), Puna Austral, *in* Actas, 16th Congreso Geológico Argentino, Volumen 1: Buenos Aires, Argentina, Asociación Geológica Argentina, p. 851–858.

Arnosio, M., Becchio, R., Viramonte, J.G., de Silva, S., and Viramonte, J.M., 2008, Geocronología e isotopía del Complejo Volcánico Cerro Blanco: Un sistema de calderas cuaternario (73–12 ka) en los Andes Centrales del sur, *in* Actas, 17th Congreso Geológico Argentino, Volumen 1: Buenos Aires, Argentina, Asociación Geológica Argentina, p. 177–178.

Báez, W., Arnosio, M., Chiodi, A., Ortiz Yañes, A., Viramonte, J.G., Bustos, E., Giordano, G., and López, J.F., 2015, Estratigrafía y evolución del Complejo Volcánico Cerro Blanco, Puna Austral, Argentina: Revista Mexicana de Ciencias Geológicas, v. 32, no. 1, p. 29–49.

Baez, W., Chiodi, A., Bustos, E., Arnosio, M., Viramonte, J.G., and Giordano, G., 2017, Mecanismos de emplazamiento y destruccion de los domos lavicos asociados a la Caldera del Cerro Blanco, Puna Austra: Revista de la Asociación Geológica Argentina, v. 74, p. 223–238.

Báez, W., de Silva, S.L., Chiodi, A., Bustos, E., Giordano, G., Arnosio, M., Suzaño, N., Viramonte, J.G., Norini, G., and Groppelli, G., 2020a, Pulsating flow dynamics of sustained, forced pyroclastic density currents: Insights from a facies analysis of the Campo de la Piedra Pómez ignimbrite, southern Puna, Argentina: Bulletin of Volcanology, v. 82, p. 53, https://doi.org/10.1007/s00445-020-01385-5.

Báez, W., Bustos, E., Chiodi, A., Reckziegel, F., Arnosio, M., de Silva, S., Giordano, G., Viramonte, J.G., Sampietro-Vattuone, M.M., and Peña-Monné., J.L., 2020b, Eruptive style and flow dynamics of the pyroclastic density currents related to the Holocene Cerro Blanco eruption (southern Puna plateau, Argentina): Journal of South American Earth Sciences, v. 98, 102482, https://doi.org/10.1016/j.jsames.2019.102482.

Bardelli, L., Arnosio, M., Báez, W., Suzaño, N., Becchio, R., Viramonte, J., Bustos, E., and Bertea, E., 2020, Multi-banded pumice in the Campo de la Piedra Pómez rhyolitic ignimbrite (southern Puna Plateau): Pre-eruptive physical and chemical interactions between mafic and rhyolitic melts: Journal of South American Earth Sciences, v. 101, 102616, https://doi.org/10.1016/j.jsames.2020.102616.

Becchio, R., Lucassen, F., Franz, G., Viramonte, J., and Wemmer, K., 1999, El basamento Paleozoico inferior del noroeste de Argentina (23° to 27°S): Metamorfismo y geocronologia, *in* Bonorino, G.G., Omarini, R., and Viramonte, J., eds., Geologia del Noroeste Argentino: XIV Congreso Geológico Argentino, Tomo I: Salta, Argentina, Asociación Geológica Argentina, p. 58–72.

Bindeman, I., 2008, Oxygen isotopes in mantle and crustal magmas as revealed by single crystal analysis: Reviews in Mineralogy and Geochemistry, v. 69, p. 445–478, https://doi.org/10.2138/rmg.2008.69.12.

Blundy, J., and Cashman, K., 2001, Ascent-driven crystallisation of dacite magmas at Mount St. Helens, 1980–1986: Contributions to Mineralogy and Petrology, v. 140, no. 6, p. 631–650, https://doi.org/10.1007/s004100000219.

Blundy, J., Cashman, K., and Humphreys, M., 2006, Magma heating by decompression-driven crystallization beneath andesite volcanoes: Nature, v. 443, p. 76–80, https://doi.org/10.1038/nature05100.

Bowen, N.L., 1937, Recent high-temperature research on silicates and its significance in igneous geology: American Journal of Science, v. 33, p. 1–21, https://doi.org/10.2475/ajs.s5-33.193.1.

Brandmeier, M., and Wörner, G., 2016, Compositional variations of ignimbrite magmas in the Central Andes over the past 26 Ma—A multivariate statistical perspective: Lithos, v. 262, p. 713–728, https://doi.org/10.1016/j.lithos.2016.07.011.

Burns, D.H., de Silva, S.L., Tepley, F.J., III, and Schmitt, A.K., 2019, Chasing the mantle: Deciphering cryptic mantle signals through Earth's thickest continental magmatic arc: Earth and Planetary Science Letters, v. 531, p. 115985, https://doi.org/10.1016/j.epsl.2019.115985.

Bustos, E., Báez, W., Norini, G., Arnosio, J.M., and de Silva, S., 2019, The geological and structural evolution of the long-lived Miocene–Pleistocene La Hoyada volcanic complex in the geodynamic framework of the Central Andes, Argentina: Journal of Volcanology and Geothermal Research, v. 385, p. 120–142, https://doi.org/10.1016/j.jvolgeores.2018.07.010.

Carr, M.J., and Gazel, E., 2017, Igpet software for modeling igneous processes: Examples of application using the open educational version: Mineralogy and Petrology, v. 111, p. 283–289, https://doi.org/10.1007/s00710-016-0473-z.

Chiodi, A., Tassi, F., Báez, W., Filipovich, R., Bustos, E., Glok Galli, M., Suzaño, N., Ahumada, M.F., Viramonte, J.G., Giordano, G., Pecoraino, G., and Vaselli, O., 2019, Preliminary conceptual model of the Cerro Blanco caldera-hosted geothermal system (southern Puna, Argentina): Inferences from geochemical investigations: Journal of South American Earth Sciences, v. 94, 102213, https://doi.org/10.1016/j.jsames.2019.102213.

Davidson, J., Turner, S., and Plank, T., 2012, Dy/Dy*: Variations arising from mantle sources and petrogenetic processes: Journal of Petrology, v. 54, no. 3, p. 525–537, https://doi.org/10.1093/petrology/egs076.

Davidson, J.P., Harmon, R.S., and Wörner, G., 1991, The source of central Andean magmas; some considerations, *in* Harmon, R.S., and Rapela, C.W., eds., Andean Magmatism and Its Tectonic Setting: Geological Society of America Special Paper 265, p. 233–244, https://doi.org/10.1130/SPE265-p233.

Deino, A., and Potts, R., 1992, Age-probability spectra for examination of single-crystal dating results: Examples from Olorgesailie, southern Kenya Rift: Quaternary International, v. 13–14, p. 47–53, https://doi.org/10.1016/1040-6182(92)90009-Q.

de Silva, S., 2008, Arc magmatism, calderas, and supervolcanoes: Geology, v. 36, p. 671–672, https://doi.org/10.1130/focus082008.1.

de Silva, S.L., 1989, The Altiplano–Puna volcanic complex of the Central Andes: Geology, v. 17, p. 1102–1106, https://doi.org/10.1130/0091-7613(1989)017<1102:APVCOT>2.3.CO;2.

de Silva, S.L., and Francis, P.W., 1991, Volcanoes of the Central Andes: Heidelberg, Germany, Springer-Verlag, 216 p.

de Silva, S.L., and Gregg, P.M., 2014, Thermomechanical feedbacks in magmatic systems: Implications for growth, longevity, and evolution of large caldera-forming magma reservoirs and their supereruptions: Journal of Volcanology and Geothermal Research, v. 282, p. 77–91, https://doi.org/10.1016/j.jvolgeores.2014.06.001.

de Silva, S.L., and Kay, S.M., 2018, Turning up the heat: High-flux magmatism in the Central Andes: Elements, v. 14, no. 4, p. 245–250, https://doi.org/10.2138/gselements.14.4.245.

de Silva, S.L., and Wolff, J.A., 1995, Zoned magma chambers: The influence of magma chamber geometry on sidewall convective fractionation: Journal of Volcanology and Geothermal Research, v. 65, no. 1–2, p. 111–118, https://doi.org/10.1016/0377-0273(94)00105-P.

de Silva, S.L., Zandt, G., Trumbull, R., Viramonte, J., Salas, G., and Jimenez, N., 2006, Large ignimbrite eruptions and volcano-tectonic depressions in the Central Andes: A thermomechanical perspective, *in* Troise, C., De Natale, G., and Kilburn, C.R.J., eds., Mechanisms of Activity and Unrest at Large Calderas: Geological Society [London] Special Publication 269, p. 47–64, https://doi.org/10.1144/GSL.SP.2006.269.01.04.

DePaolo, D.J., 1981, Trace element and isotopic effects of combined wallrock assimilation and fractional crystallization: Earth and Planetary Science Letters, v. 53, p. 189–202, https://doi.org/10.1016/0012-821X(81)90153-9.

Drew, S.T., Ducea, M.N., and Schoenbohm, L.M., 2009, Mafic volcanism on the Puna Plateau, NW Argentina: Implications for lithospheric composition and evolution with an emphasis on lithospheric foundering: Lithosphere, v. 1, no. 5, p. 305–318, https://doi.org/10.1130/L54.1.

Fernández-Turiel, J.L., Perez-Torrado, F.J., Rodríguez González, A., Saavedra, J., Carracedo, J.C., Rejas, M., Lobo, A., Osterrieth, M., Carrizo, J., Esteban, G., Gallardo, J., and Ratto, N., 2019, The large eruption 4.2 ka cal BP in Cerro Blanco, Central volcanic zone, Andes: Insights to the Holocene eruptive deposits in the southern Puna and adjacent regions: Estudios Geológicos, v. 718, e088, https://doi.org/10.3989/egeol.43438.515.

Folkes, C.B., Wright, H.M., Cas, R.A.F., de Silva, S.L., Lesti, C., and Viramonte, J.G., 2011a, A reappraisal of the stratigraphy and volcanology of the Cerro Galán volcanic system, NW Argentina: Bulletin of Volcanology, v. 73, p. 1427–1454, https://doi.org/10.1007/s00445-011-0459-y.

Folkes, C.B., de Silva, S.L., Schmitt, A.K., and Cas, R.A.F., 2011b, A reconnaissance of U-Pb zircon ages in the Cerro Galán system, NW Argentina: Prolonged magma residence, crystal recycling, and crustal assimilation: Journal of Volcanology and Geothermal Research, v. 206, p. 136–147, https://doi.org/10.1016/j.jvolgeores.2011.06.001.

Folkes, C.B., Silva, S.L., Wright, H.M., and Cas, R.A.F., 2011c, Geochemical homogeneity of a long-lived, large silicic system: Evidence from the Cerro Galán caldera, NW Argentina: Bulletin of Volcanology, v. 73, no. 10, p. 1455–1486, https://doi.org/10.1007/s00445-011-0511-y.

Folkes, C.B., de Silva, S.L., Bindeman, I.N., and Cas, R.A., 2013, Tectonic and climate history influence the geochemistry of large-volume silicic magmas: New $\delta^{18}O$ data from the Central Andes with comparison to N America and Kamchatka: Journal of Volcanology and Geothermal Research, v. 262, p. 90–103, https://doi.org/10.1016/j.jvolgeores.2013.05.014.

Francis, P.W., Sparks, R.S.J., Hawkesworth, C.J., Thorpe, R.S., Pyle, D.M., Tait, S.R., Mantovani, M.S.M., and McDermott, F., 1989, Petrology and geochemistry of volcanic rocks of the Cerro Galan caldera, northwest Argentina: Geological Magazine, v. 126, p. 515–547, https://doi.org/10.1017/S0016756800022834.

Freymuth, H., Brandmeier, M., and Wörner, G., 2015, The origin and crust/mantle mass balance of Central Andean ignimbrite magmatism constrained by oxygen and strontium isotopes and erupted volumes: Contributions to Mineralogy and Petrology, v. 169, 58, https://doi.org/10.1007/s00410-015-1152-5.

Gardner, J.E., Befus, K.S., Gualda, G.A.R., and Ghiorso, M.S., 2014, Experimental constraints on rhyolite-MELTS and the late Bishop Tuff magma body: Contributions to Mineralogy and Petrology, v. 168, no. 2, 1051, https://doi.org/10.1007/s00410-014-1051-1.

Goss, A.R., and Kay, S.M., 2009, Extreme high field strength element (HFSE) depletion and near-chondritic Nb/Ta ratios in Central Andean adakite-like lavas (~28°S, ~68°W): Earth and Planetary Science Letters, v. 279, no. 1–2, p. 97–109, https://doi.org/10.1016/j.epsl.2008.12.035.

Goss, A.R., Kay, S.M., Mpodozis, C., and Singer, B.S., 2009, The Incapillo caldera and dome complex (~28°S, Central Andes): A stranded magma chamber over a dying arc: Journal of Volcanology and Geothermal Research, v. 184, p. 389–404, https://doi.org/10.1016/j.jvolgeores.2009.05.005.

Goss, A.R., Kay, S.M., and Mpodozis, C., 2010, The geochemistry of a dying continental arc: The Incapillo caldera and dome complex of the southernmost Central Andean volcanic zone (~28°S): Contributions to Mineralogy and Petrology, v. 161, no. 1, p. 101–128, https://doi.org/10.1007/s00410-010-0523-1.

Grocke, S.B., Cottrell, E., de Silva, S., and Kelley, K.A., 2016, The role of crustal and eruptive processes versus source variations in controlling the oxidation state of iron in Central Andean magmas: Earth and Planetary Science Letters, v. 440, no. C, p. 92–104, https://doi.org/10.1016/j.epsl.2016.01.026.

Grocke, S.B., Andrews, B.J., and de Silva, S.L., 2017a, Experimental and petrological constraints on long-term magma dynamics and post-climactic eruptions at the Cerro Galán caldera system, NW Argentina: Journal of Volcanology and Geothermal Research, v. 347, no. C, p. 296–311, https://doi.org/10.1016/j.jvolgeores.2017.09.021.

Grocke, S.B., de Silva, S.L., Iriarte, R., Lindsay, J.M., and Cottrell, E., 2017b, Catastrophic caldera-forming (CCF) monotonous silicic magma reservoirs: Geochemical and petrological constraints on heterogeneity, magma dynamics, and eruption dynamics of the 3.49 Ma Tara supereruption, Guacha II caldera, SW Bolivia: Journal of Petrology, v. 58, no. 2, p. 227–260, https://doi.org/10.1093/petrology/egx012.

Gualda, G.A.R., and Ghiorso, M.S., 2013, Low-pressure origin of high-silica rhyolites and granites: The Journal of Geology, v. 121, no. 5, p. 537–545, https://doi.org/10.1086/671395.

Gualda, G.A.R., Ghiorso, M.S., Lemons, R.V., and Carley, T.L., 2012, Rhyolite-MELTS: A modified calibration of MELTS optimized for silica-rich, fluid-bearing magmatic systems: Journal of Petrology, v. 53, no. 5, p. 875–890, https://doi.org/10.1093/petrology/egr080.

Guzmán, S., Grosse, P., Montero López, C., Hongn, F., Pilger, R., Petrinovic, I., Seggiaro, R., and Aramayo, A., 2014, Spatial-temporal distribution of explosive volcanism in the 25–28°S segment of the Andean Central volcanic zone: Tectonophysics, v. 636, p. 170–189, https://doi.org/10.1016/j.tecto.2014.08.013.

Haag, M.B., Báez, W.A., Sommer, C.A., Arnosio, J.M., and Filipovich, R.E., 2019, Geomorphology and spatial distribution of monogenetic volcanoes in the southern Puna Plateau (NW Argentina): Geomorphology, v. 342, p. 196–209, https://doi.org/10.1016/j.geomorph.2019.06.008.

Henderson, S., and Pritchard, M.E., 2013, Decadal volcanic deformation in the Central Andes volcanic zone revealed by InSAR time series: Geochemistry Geophysics Geosystems, v. 14, p. 1358–1374, https://doi.org/10.1002/ggge.20074.

Hildreth, E.W., 1981, Gradients in silicic magma chambers: Implications for lithospheric magmatism: Journal of Geophysical Research, v. 86, p. 10153–10192, https://doi.org/10.1029/JB086iB11p10153.

Isacks, B.L., 1988, Uplift of the Central Andean Plateau and bending of the Bolivian orocline: Journal of Geophysical Research, v. 93, no. B4, p. 3211–3231, https://doi.org/10.1029/JB093iB04p03211.

Johannes, W., and Holtz, F., 1996, Petrogenesis and Experimental Petrology of Granitic Rocks: Berlin, Springer, 335 p., https://doi.org/10.1007/978-3-642-61049-3.

Johnson, D., Hooper, P., and Conrey, R., 1999, XRF analysis of rocks and minerals for major and trace elements on a single low dilution Li-tetraborate fused bead: Advances in X-Ray Analysis, v. 41, p. 843–867.

Kay, S.M., and Coira, B.L., 2009, Shallowing and steepening subduction zones, continental lithospheric loss, magmatism, and crustal flow under the central Andean Altiplano-Puna Plateau, *in* Kay, S.M., Ramos, V.A., and Dickinson, W.R., eds., Backbone of the Americas: Shallow Subduction, Plateau Uplift, and Ridge and Terrane Collision: Geological Society of America Memoir 204, p. 229–260, https://doi.org/10.1130/2009.1204(11).

Kay, S.M., Mpodozis, C., Ramos, V.A., and Munizaga, F., 1991, Magma source variations for mid–late Tertiary magmatic rocks associated with a shallowing subduction zone and a thickening crust in the Central Andes (28 to 33°S), *in* Harmon, R.S., and Rapela, C.W., eds., Andean Magmatism and Its Tectonic Setting: Geological Society of America Special Paper 265, p. 113–138, https://doi.org/10.1130/SPE265-p113.

Kay, S.M., Coira, B., and Viramonte, J., 1994, Young mafic back arc volcanic rocks as indicators of continental lithospheric delamination beneath the Argentine Puna plateau, central Andes: Journal of Geophysical Research, v. 99, no. B12, p. 24323–24339, https://doi.org/10.1029/94JB00896.

Kay, S.M., Coira, B.L., Caffe, P.J., and Chen, C.-H., 2010a, Regional chemical diversity, crustal and mantle sources and evolution of central Andean Puna plateau ignimbrites: Journal of Volcanology and Geothermal Research, v. 198, p. 81–111, https://doi.org/10.1016/j.jvolgeores.2010.08.013.

Kay, S.M., Coira, B., Wörner, G., Kay, R.W., and Singer, B.S., 2010b, Geochemical, isotopic and single crystal $^{40}Ar/^{39}Ar$ age constraints on the evolution of the Cerro Galán ignimbrites: Bulletin of Volcanology, v. 73, no. 10, p. 1487–1511, https://doi.org/10.1007/s00445-010-0410-7.

Kent, A.J.R., Stolper, E.M., Francis, D., Woodhead, J., Frei, R., and Eiler, J., 2004, Mantle heterogeneity during the formation of the North Atlantic igneous province: Constraints from trace element and Sr-Nd-Os-O isotope systematics of Baffin Island picrites: Geochemistry Geophysics Geosystems, v. 5, Q11004, https://doi.org/10.1029/2004GC000743.

Koppers, A., 2002, ArArCALC—Software for $^{40}Ar/^{39}Ar$ age calculations: Computers & Geosciences, v. 28, no. 5, p. 605–619, https://doi.org/10.1016/S0098-3004(01)00095-4.

Lange, R.A., Frey, H.M., and Hector, J., 2009, A thermodynamic model for the plagioclase-liquid hygrometer/thermometer: The American Mineralogist, v. 94, p. 494–506, https://doi.org/10.2138/am.2009.3011.

Le Bas, M.J., LeMaitre, R.W., and Streckeisen, A., 1986, A chemical classification of volcanic rocks based on the total alkali-silica diagram: Journal of Petrology, v. 27, p. 745–750, https://doi.org/10.1093/petrology/27.3.745.

Le Maitre, R.W., 1984, A proposal by the IUGS Subcommission on the Systematics of Igneous Rocks for a chemical classification of volcanic rocks based on the total alkali silica (TAS) diagram: Australian Journal of Earth Sciences, v. 31, p. 243–255.

Lindsay, J.M., Schmitt, A.K., Trumbull, R.B., de Silva, S.L., Siebel, W., and Emmermann, R., 2001, Magmatic evolution of the La Pacana caldera system, Central Andes, Chile: Compositional variation of two cogenetic, large-volume felsic ignimbrites: Journal of Petrology, v. 42, p. 459–486, https://doi.org/10.1093/petrology/42.3.459.

Lowenstern, J., 1995, Applications of silicate-melt inclusions to the study of magmatic volatiles, *in* Thompson, J.F.H., ed., Magmas, Fluids and Ore Deposits: Mineralogical Association of Canada Short Course Series 23, p. 71–99.

Lozano, R., and Bernal, J.-P., 2005, Characterization of a new set of eight geochemical reference materials for XRF major and trace element analysis: Revista Mexicana de Ciencias de la Tierra, v. 3, p. 329–344.

Lucassen, F., Becchio, R., Harmon, R., Kasemann, S., Franz, G., Trumbull, R., Wilke, H., Romer, R.L., and Dulski, R., 2001, Composition and density model of the continental crust at an active continental margin—The Central Andes between 21° and 27°S: Tectonophysics, v. 341, no. 1, p. 195–223, https://doi.org/10.1016/S0040-1951(01)00188-3.

Maro, G., Caffe, P.J., Romer, R.L., and Trumbull, R.B., 2017, Neogene mafic magmatism in the northern Puna Plateau, Argentina: Generation and evolution of a back-arc volcanic suite: Journal of Petrology, v. 58, no. 8, p. 1591–1617, https://doi.org/10.1093/petrology/egx066.

Michael, P.J., 1983, Chemical differentiation of the Bishop Tuff and other high-silica magmas through crystallization processes: Geology, v. 11, p. 31–34, https://doi.org/10.1130/0091-7613(1983)11<31:CDOTBT>2.0.CO;2.

Miller, C.F., and Mittlefehldt, D.W., 1984, Extreme fractionation in felsic magma chamber: A product of liquid state differentiation or fractional crystallization?: Earth and Planetary Science Letters, v. 68, p. 151–158, https://doi.org/10.1016/0012-821X(84)90147-X.

Montero López, M.C., Hongn, F.D., Seggiaro, R., Marrett, R., and Ratto, N., 2009, Relación entre el volcanismo y los registros arqueológicos en el bolsón de Fiambalá, *in* Ratto, N., compiler, Entrelazando Ciencias, Sociedad y Ambiente Antes de la Conquista Española: Buenos Aires, Argentina, EUDEBA, p. 131–156.

Montero López, M.C., Hongn, F., Brod, J.A., Seggiaro, R., Marrett, R., and Sudo, M., 2010a, Magmatismo ácido del Mioceno Superior–Cuaternario en el área de Cerro Blanco–La Hoyada, Puna Sur: Revista de la Asociación Geológica Argentina, v. 67, no. 3, p. 329–348.

Montero López, M.C., Hongn, F., Marrett, R., Seggiaro, R., Strecker, M., and Sudo, M., 2010b, Late Miocene–Pliocene onset of N-S extension along the southern margin of the Central Andean Puna plateau from magmatic, geochronological and structural evidences: Tectonophysics, v. 494, p. 48–63, https://doi.org/10.1016/j.tecto.2010.08.010.

Montero López, M.C., Strecker, M.R., Schildgen, T.F., Hongn, F., Guzmán, S., Bookhagen, B., and Sudo, M., 2014, Local high relief at the southern margin of the Andean plateau by 9 Ma: Evidence from ignimbritic valley fills and river incision: Terra Nova, v. 26, no. 6, p. 454–460, https://doi.org/10.1111/ter.12120.

Montero López, M.C., Guzman, S., and Barrios, F., 2015, Late Miocene ignimbrites at the southern Puna–northern Sierras Pampeanas border (27°S): Stratigraphic correlation: Journal of South American Earth Sciences, v. 62, p. 80–91, https://doi.org/10.1016/j.jsames.2015.05.004.

Naranjo, J.A., Villa, V., Ramírez, C., and Pérez de Arce, C., 2018, Volcanism and tectonism in the southern Central Andes: Tempo, styles, and relationships: Geosphere, v. 14, no. 2, p. 626–641, https://doi.org/10.1130/GES01350.1.

Nielsen, C., and Sigurdsson, H., 1981, Quantitative methods for electron microprobe analysis of sodium in natural and synthetic glasses: The American Mineralogist, v. 66, p. 547–552.

Norini, G., Cogliati, S., Baez, W., Arnosio, M., Bustos, E., Viramonte, J., and Groppelli, G., 2014, The geological and structural evolution of the Cerro Tuzgle Quaternary stratovolcano in the back-arc region of the Central Andes, Argentina: Journal of Volcanology and Geothermal Research, v. 285, p. 214–228, https://doi.org/10.1016/j.jvolgeores.2014.08.023.

Okumura, S., de Silva, S.L., Nakamura, M., and Osamu, S., 2019, Caldera-forming eruptions of mushy magma modulated by feedbacks between ascent rate, gas retention/loss and bubble/crystal framework interaction: Scientific Reports, v. 9, no. 1, p. 15845, https://doi.org/10.1038/s41598-019-52272-9.

Pallister, J.S., Thornber, C.R., Cashman, K.V., Clynne, M.A., Lowers, H.A., Mandeville, C.A., Brownfield, I.K., and Meeker, G.P., 2008, Petrology of the 2004–2006 Mount St. Helens Lava Dome—Implications for Magmatic Plumbing and Eruption Triggering: U.S. Geological Society Professional Paper 750, p. 647–702, https://doi.org/10.3133/pp175030.

Petrinovic, I.A., Riller, U., Brod, J.A., Alvarado, G., and Arnosio, M., 2006, Bimodal volcanism in a tectonic transfer zone: Evidence for tectonically controlled magmatism in the southern Central Andes, NW Argentina: Journal of Volcanology and Geothermal Research, v. 152, no. 3–4, p. 240–252, https://doi.org/10.1016/j.jvolgeores.2005.10.008.

Ramos, F.C., 1992, Isotope Geology of the Metamorphic Core of the Central Grouse Creek Mountains, Box Elder County, Utah [Ph.D. dissertation]:, Los Angeles, California, University of California–Los Angeles, 300 p.

Riller, U., Petrinovic, I., Ramelow, J., Strecker, M., and Oncken, O., 2001, Late Cenozoic tectonism, collapse caldera and plateau formation in the Central Andes: Earth and Planetary Science Letters, v. 188, p. 299–311, https://doi.org/10.1016/S0012-821X(01)00333-8.

Risse, A., Trumbull, R.B., Coira, B., Kay, S.M., and van den Bogaard, P., 2008, $^{40}Ar/^{39}Ar$ geochronology of mafic volcanism in the back-arc region of the southern Puna plateau, Argentina: Journal of South American Earth Sciences, v. 26, no. 1, p. 1–15, https://doi.org/10.1016/j.jsames.2008.03.002.

Risse, A., Trumbull, R.B., Kay, S.M., Coira, B., and Romer, R.L., 2013, Multi-stage evolution of late Neogene mantle-derived magmas from the Central Andes back-arc in the southern Puna Plateau of Argentina: Journal of Petrology, v. 54, no. 10, p. 1963–1995, https://doi.org/10.1093/petrology/egt038.

Roberge, J., de Silva, S., Arnosio, M., Becchio, R., and Viramonte, J.G., 2018, Magmatic architecture and dynamics of the Cerro Blanco volcanic complex, Catamarca, Argentina: Goldschmidt Conference Abstracts, v. 2018, abstract 2165.

Rutherford, M.J., and Hill, P.M., 1993, Magma ascent rates from amphibole breakdown: An experimental study applied to the 1980–1986 Mount St. Helens eruption: Journal of Geophysical Research, v. 98, p. 19667–19685, https://doi.org/10.1029/93JB01613.

Salisbury, M.J., Jicha, B.R., de Silva, S.L., Singer, B.S., Jimenez, N.C., and Ort, M.H., 2011, $^{40}Ar/^{39}Ar$ chronostratigraphy of Altiplano-Puna volcanic complex ignimbrites reveals the development of a major magmatic province: Geological Society of America Bulletin, v. 123, p. 821–840, https://doi.org/10.1130/B30280.1.

Schmitt, A.K., de Silva, S.L., Trumbull, R.B., and Emmermann, R., 2001, Magma evolution in the Purico ignimbrite complex, northern Chile: Evidence for zoning of a dacitic magma by injection

of rhyolitic melts following mafic recharge: Contributions to Mineralogy and Petrology, v. 140, p. 680–700, https://doi.org/10.1007/s004100000214.

Schnurr, W.B.W., Trumbull, R.B., Clavero, J., Hahne, K., Siebel, W., and Gardeweg, M., 2007, Twenty-five million years of silicic volcanism in the southern Central volcanic zone of the Andes: Geochemistry and magma genesis of ignimbrites from 25 to 27 degrees S, 67 to 72 degrees W: Journal of Volcanology and Geothermal Research, v. 166, p. 17–46, https://doi.org/10.1016/j.jvolgeores.2007.06.005.

Seggiaro, R., Hongn, F., Folguera, A. Clavero, J., 2000, Hoja Geológica 2769—II. Paso de San Francisco: Servicio Geológico Minero Argentino (SEGEMAR), Programa Nacional de Cartas Geológicas Boletín 294, scale 1:250,000.

Siebel, W., Schnurr, W.B.W., Hahne, K., Kraemer, B., Trumbull, R.B., van den Bogaard, P., and Emmermann, R., 2001, Geochemistry and isotope systematics of small- to medium-volume Neogene–Quaternary ignimbrites in the southern central Andes: Evidence for derivation from andesitic magma sources: Chemical Geology, v. 171, p. 213–237, https://doi.org/10.1016/S0009-2541(00)00249-7.

Sparks, R.S.J., Francis, P.W., Hamer, R.D., Pankhurst, R.J., O'Callaghan, L.J., Thorpe, R.S., and Page, R., 1985, Ignimbrites of the Cerro Galan caldera, NW Argentina: Journal of Volcanology and Geothermal Research, v. 24, p. 205–248, https://doi.org/10.1016/0377-0273(85)90071-X.

Stormer, J.C., and Nicholls, J., 1978, XLFRAC: A program for the interactive testing of magmatic differentiation models: Computers & Geosciences, v. 4, no. 2, p. 143–159, https://doi.org/10.1016/0098-3004(78)90083-3.

Sun, S., and McDonough, W.F., 1989, Chemical and isotopic systematics of oceanic basalts: Implications for mantle composition and processes, *in* Saunders, A.D., and Norry, M.J., eds., Magmatism in the Ocean Basins: Geological Society [London] Special Publication 42, p. 313–345, https://doi.org/10.1144/GSL.SP.1989.042.01.19.

Taylor, S.R., and McLennan, S.M., 1985, The Continental Crust: Its Composition and Evolution: Oxford, UK, Blackwell, 312 p.

Tepley, F.J., de Silva, S.L., and Salas, G., 2013, Magma dynamics and petrological evolution leading to the VEI 5 2000 B.P. eruption of El Misti Volcano, southern Peru: Journal of Petrology, v. 54, p. 2033–2065, https://doi.org/10.1093/petrology/egt040.

Thorpe, R.S., Francis, P.W., and O'Callaghan, L.J., 1984, Relative roles of source composition, fractional crystallization and crustal contamination in the petrogenesis of Andean volcanic rocks: Philosophical Transactions of the Royal Society of London A—Mathematical and Physical Sciences, v. 310, p. 675–692.

Trumbull, R.B., Wittenbrink, R., and Hahne, K., 1999, Evidence for late Miocene to recent contamination of arc andesites by crustal melts in the Chilean Andes (25–26°S) and its geodynamic implications: Journal of South American Earth Sciences, v. 12, no. 2, p. 135–155, https://doi.org/10.1016/S0895-9811(99)00011-5.

Tuttle, O.F., and Bowen, N.L., 1958, Origin of Granite in the Light of Experimental Studies in the System $NaAlSi_3O_8$-$KAlSi_3O_8$-SiO_2-H_2O: Geological Society of America Memoir 74, 153 p., https://doi.org/10.1130/MEM74.

Viramonte, J.G., and Petrinovic, I.A., 1990, Calderas asociadas a megafracturas transcurrentes en los Andes Centrales del Sur, *in* Actas, 11th Congreso Geologico Argentino, Volumen 2: Buenos Aires, Argentina, Asociación Geológica Argentina, p. 369–372.

Viramonte, J.G., Galliski, M.A., Araia Saavedra, V., Aparicio, A., Garcia Cucho, L., and Martin Escorza, C., 1984, El finivulcanismo basico de la depresion de Arizaro, provincia de Salta, *in* Actas, 9th Congreso Geologico Argentino, Volumen 3: Buenos Aires, Argentina, Asociación Geológica Argentina, p. 234–251.

Viramonte, J.G., Castro Godoy, S., Arnosio, J.M., Becchio, R., and Poodts, M., 2005, El Campo Geotermal de la Caldera de Cerro Blanco, utilización de imágenes Aster, *in* Acta, Congreso Geológico Argentino, Septiembre 2005, Volumen II: La Plata, Argentina, Asociación Geológica Argentina, p. 505–512.

Williams, H., and McBirney, A.R., 1979, Volcanology: San Francisco, California, Freeman, Cooper and Co., 397 p.

Wolff, J.A., and Ramos, F.C., 2003, Pb-isotope variations among Bandelier Tuff feldspars: No evidence for a long-lived silicic magma chamber: Geology, v. 31, p. 533–536, https://doi.org/10.1130/0091-7613(2003)031<0533:PIVABT>2.0.CO;2.

Wolff, J.A., Worner, G., and Blake, S., 1990, Gradients in physical parameters in zoned magmatic systems: Implications for evolution and eruptive withdrawal: Journal of Volcanology and Geothermal Research, v. 43, p. 37–55, https://doi.org/10.1016/0377-0273(90)90043-F.

Wright, H.M.N., Folkes, C.B., Cas, R.A.F., and Cashman, K.V., 2011, Heterogeneous pumice populations in the 2.08-Ma Cerro Galán ignimbrite: Implications for magma recharge and ascent preceding a large-volume silicic eruption: Bulletin of Volcanology, v. 73, no. 10, p. 1513–1533, https://doi.org/10.1007/s00445-011-0525-5 .